RAA 2020 Vol. **20** No. **10**, 163(20pp) doi: 10.1088/1674-4527/20/10/163

http://www.raa-journal.org *http://iopscience.iop.org/raa*

Research in Astronomy and Astrophysics

Contact binaries at different evolutionary stages

Sheng-Bang Qian[1,2,3,4,5], Li-Ying Zhu[1,3,4,5], Liang Liu[1,3,4,5], Xu-Dong Zhang[1,3,4,5], Xiang-Dong Shi[1,3,4], Jia-Jia He[1,3,4] and Jia Zhang[1,3,4]

1 Yunnan Observatories, Chinese Academy of Sciences, Kunming 650216, China; *qsb@ynao.ac.cn*
2 School of Physics and Astronomy, Yunnan University, Kunming 650091, China
3 Key Laboratory for the Structure and Evolution of Celestial Objects, Chinese Academy of Sciences, Kunming 650216, China
4 Center for Astronomical Mega-Science, Chinese Academy of Sciences, Beijing 100101, China
5 University of Chinese Academy of Sciences, Beijing 100049, China

Received 2020 August 17; accepted 2020 August 31

Abstract Contact binaries consist of two strongly interacting component stars where they are filling their critical Roche lobes and sharing a common envelope. Most of them are main-sequence stars, but some of them are post main-sequence systems. They are good astrophysical laboratories for studying several problems such as the merging of binary stars, evolution of the common envelope, the origin of luminous red nova outbursts and the formation of rapidly rotating single stars with possible planetary systems. A large number of contact binary candidates were detected by several photometric surveys around the world and many of them were observed by the LAMOST spectroscopic survey. Based on follow-up observations, the evolutionary states and geometrical structures of some systems were understood well. In this review, we will introduce and catalog new stellar atmospheric parameters (i.e., the effective temperature ($T_{\rm eff}$), the gravitational acceleration ($\log(g)$), metallicity ([Fe/H]) and radial velocity (V_r)) for 9149 EW-type contact binaries that were obtained based on low- and medium-resolution spectroscopic surveys of LAMOST. Then we will focus on several groups of contact binary stars, i.e., marginal contact binary systems, deep and low-mass ratio contact binary stars, binary systems below the short-period limit of contact binaries and evolved contact binaries. Marginal contact binaries are at the beginning of the contact stage, while deep and low-mass ratio contact binary stars are at the final evolutionary stage of tidally locked binaries. Several statistical relations including the period-temperature relation are determined well by applying LAMOST data and their formation and evolutionary states are reviewed. The period-color relation of M-type binaries reveals that there are contact binaries below the short-period limit. Searching for and investigating contact binaries near and below this limit will help us to understand the formation of contact binary systems and a new prediction for the short-period limit is about 0.15 d. Some evolved contact binaries were detected by the LAMOST survey where both components are sub-giants or giants. They provide a good opportunity to investigate evolution of the common envelope and are the progenitors of luminous red novae like V1309 Sco.

Key words: binaries: eclipsing — stars: late-type — stars: low-mass — stars: formation — stars: evolution

1 INTRODUCTION

A contact binary is a close binary system in which both components fill their Roche lobes (RLs, Kopal 1959) and share a common envelope (CE). Energy is transferring from the primary (the hotter one) to the secondary (the cooler one) through the CE and causes the two components to have nearly the same temperature even though their masses are quite different (Lucy 1968b,a). Because of these properties, they show an EW-type light curve where the light variation is continuous and the depths of the primary and secondary minima in the light curve are almost equal (Samus' et al. 2017). The orbital periods of most EW-type binaries are shorter than one day and they follow the famous period-color relation (Eggen 1967; Rucinski 1998). In the past two decades, a large number of EW-type contact binaries were discovered by several photometric surveys, such as the All Sky Automated Survey (ASAS, Pojmanski 1997; Pojmanski et al. 2005), Sloan Digital Sky Survey (SDSS, York et al. 2000), Northern Sky Variability Survey (NSVS, Woźniak et al. 2004), HATNet Survey (Bakos et al. 2004), SuperWASP (Pollacco et al. 2006), Catalina Sky Survey (CSS, Drake et al. 2009, 2014), Kepler Space Telescope (Borucki et al. 2010), KELT survey (Pepper et al. 2012), asteroid survey LINEAR (Palaversa et al. 2013) and K2 mission (Howell et al. 2014). In the catalog of VSX[1] (Watson et al. 2006), 86 384 EW-type binary systems were listed by 2020 August 3.

The orbital period distribution of contact binaries is another very important character that has been investigated by several authors (e.g., Lucy 1976; Rucinski 1992, 2007; Qian et al. 2017). The distribution usually has a strong maximum and a very sharp edge at about 0.22 d, i.e., the short-period limit of contact binaries. The maximum in the period distribution was determined to be about 0.35 d by Lucy (1976) and Rucinski (1992), while a maximum located at a shorter period (about 0.37 d) was given by Paczyński et al. (2006) who analyzed EWs in ASAS. Recently, Qian et al. (2017) obtained a period distribution by considering the orbital periods of 40 464 EWs collected in VSX by 2017 March 13. The maximum of the distribution is determined at about 0.29 d. The new period distribution based on 86 384 EW-type contact binaries listed in VSX by 2020 August 3 is shown in Figure 1. As displayed in the figure, the maximum of the distribution is at about 0.31 d and most EWs are in the orbital period range from 0.285 to 0.345 d.

Thanks to a series of radial velocity studies of close binary stars observed at the David Dunlap Observatory (Lu & Rucinski 1999; Lu et al. 2001; Rucinski & Lu 1999; Rucinski et al. 2000, 2001, 2002, 2003, 2005, 2008; Pych et al. 2004, Pribulla et al. 2006, 2007, 2009b,c), radial velocity curves of 111 contact binaries (45 W-type, 66 A-type) were obtained and their spectroscopic parameters were determined. This provides a great contribution to research on contact binaries. However, among 86 384 EW-type binaries listed in the VSX, these binaries are only a very small percentage and all of them are bright targets. The spectroscopic information on EWs is still lacking. Recently, based on the Large Sky Area Multi-Object Fiber Spectroscopic Telescope (LAMOST) survey in the time interval from 2011 October 24 to 2016 November 30 (e.g., Luo et al. 2012, 2015; Zhao et al. 2012), Qian et al. (2017) published spectral types of 7938 EWs. For 5363 of them, the stellar atmospheric parameters including the effective temperature $T_{\rm eff}$, the gravitational acceleration $\log(g)$, metallicity [Fe/H] and radial velocity V_r were obtained and their physical properties were analyzed. By combining the Kepler photometric data with the LAMOST spectroscopic observations, Zhang et al. (2019) provided a catalog of 1320 binaries with plentiful parameters including 118 contact binaries and some statistical results were obtained after the corrections on selection bias. To understand the evolutionary states and geometrical structures of contact binaries well, some researchers have done follow-up studies after the LAMOST survey (e.g. Lu et al. 2017; Pi et al. 2017; Wang 2017; Wang et al. 2017; Cheng et al. 2019; Hu et al. 2019; Liao & Sarotsakulchai 2019; Long et al. 2019; Yue et al. 2019; Liu et al. 2020b; Shi et al. 2020; Zhang et al. 2020a).

There were some reviews or statistical papers about contact binaries worthy of attention. Eggen (1967) put forward a very important relationship on contact binaries, the period-color relationship. It leads to the model of thermal relaxation oscillation (TRO) (Lucy 1976; Flannery 1976; Robertson & Eggleton 1977). Rucinski (1986) discussed the effect of angular momentum loss (AML) on the formation of contact binaries. Qian (2001a,b, 2003) suggested a critical value of mass ratio (i.e. $q = 0.4$) around which the periods of contact binaries oscillate. Webbink (2003) pointed out that some problems associated with contact binaries, especially the problem of energy transfer in massive early-type contact binaries where the system should have a common radiative envelope. He also reviewed the thermal equilibrium models and TRO models. Eggleton (2012) described a series of processes, including hierarchical fragmentation, gravitational scattering, Kozai cycles within triple systems, tidal friction and magnetic braking, that are responsible for producing contact binaries. Yildiz & Doğan (2013) suggested that contact binaries that have experienced mass ratio reversal in their secondaries are overluminous. They applied a new method to compute the initial masses of contact binaries and found that binaries with initial masses higher then 1.8 solar mass become A-subtype contact binaries while binaries with initial masses lower than this value become W-subtype. Based on this work, Yıldız (2014) estimated the mean ages of A- and W-subtype contact binaries are 4.4 Gyr and 4.6 Gyr, respectively. Recently, by investigating EAs and EWs observed by LAMOST together, Qian et al. (2018) pointed out that the modern EW populations may be formed through a combination of several mechanisms.

Besides the original low-resolution spectra (LRS), LAMOST carried out a medium-resolution spectroscopic survey from September 2018 with a ∼7500 spectral resolu-

[1] http://www.aavso.org/vsx/

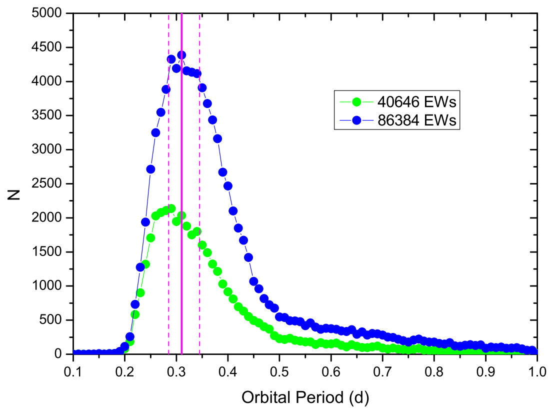

Fig. 1 Period distribution of contact binaries. Blue dots refer to the new period distribution based on 86 384 contact binaries currently listed in the VSX catalog, while green dots to an old distribution based on 40 646 systems that were listed in VSX by 2017 March 13. The peak of the new distribution is near 0.31 d (*the solid magenta line*). Most of the contact binaries are in the period range from 0.285 to 0.345 d (*the two dashed magenta lines*).

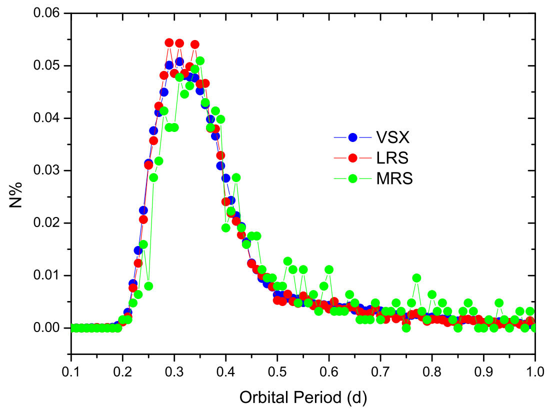

Fig. 2 Relative distribution of orbital period for contact binaries. Blue dots refer to all EW-type contact binaries listed in the VSX catalog, while red and green dots to those contact binaries whose stellar atmospheric parameters were determined by using low- and medium-resolution spectroscopic surveys from LAMOST.

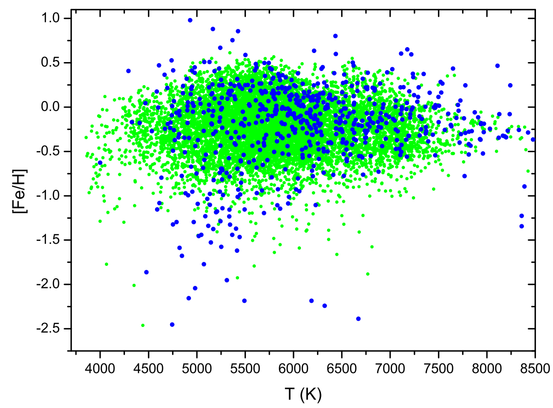

Fig. 3 Correlation between the effective temperature and metallicity [Fe/H] based on parameters of 9138 contact binaries. Green dots refer to binary stars observed in the low-resolution spectroscopic survey, while blue dots to those systems observed in the medium-resolution survey.

tion and a limiting magnitude of $G \sim 15$ mag. The medium-resolution spectrographs cover the wavelength range from 4950 Å to 5350 Å (blue camera) and from 6300 Å to 6800 Å (red camera) (Liu et al. 2020a). LAMOST plans to observe about 2 million stellar spectra, within which about 200 thousand stars will be observed 60 times on average from 2108 to 2023, called the time-domain spectroscopic survey. To get to this point, the medium-resolution survey will take up half of the telescope's observation time. In this paper, we review progresses related to the LAMOST spectroscopic survey on EW-type contact binaries observed in the time interval from 2011 October 24 to 2019 June 8. Stellar atmospheric parameters of 9149 EWs determined by low- and medium-resolution spectroscopic surveys are cataloged. Then we focus on several groups of contact binaries, i.e., marginal contact binary systems, deep and low-mass ratio contact binaries (DLMCBs), systems near and below the short-period limit of contact binaries and advanced evolved contact binary systems. Their physical properties, formation and evolutionary states are introduced and discussed based on LAMOST data together with those determined by utilizing many telescopes around the world. Finally, we give some conclusions and suggestions on future works.

2 NEW STELLAR ATMOSPHERIC PARAMETERS OF CONTACT BINARIES OBTAINED BY LAMOST

Since the investigation by Qian et al. (2017), many EW-type contact binaries were observed in the LAMOST spectroscopic survey. On 2020 May 7, data from LAMOST Data Release 7 (DR7) V1.1 were released which include observations in the time interval from 2011 October 24 to 2019 June 8. A total of 10 602 012 LRS were obtained and 9 529 826 of them are stellar spectra. Meanwhile, 3 856 218 medium-resolution stellar spectra were acquired.

Table 1 Catalog of Stellar Atmospheric Parameters for 8520 EWs Determined with LRS (the First 30 Observations)

Name (1)	R.A. (2)	Dec. (3)	Type (4)	P (d) (5)	Date (6)	Sp. (7)	T (K) (8)	E_1 (9)	log(g) (10)	E_2 (11)	[Fe/H] (12)	E_3 (13)	Vr (km s^{-1}) (14)	E_4 (15)
V0467 And	000006.52	+352200.7	EW	0.3535394	2014–12–19	G6	5650.26	58.84	4.065	0.097	0.405	0.057	–34.60	14.67
V1296 Cas	000024.52	+552748.4	EW	0.3709583	2014–11–20	G2	6002.19	202.11	4.229	0.314	0.108	0.187	–54.54	10.90
WISE J000025.3+154056	000025.31	+154056.4	EW	0.3283491	2012–09–28	G2	5853.47	74.64	4.176	0.121	–0.397	0.071	–25.74	11.99
GSC 02781–00387	000030.43	+391107.0	EW	0.2879	2013–11–14	G7	5584.36	45.12	4.353	0.074	–0.118	0.044	–19.00	10.06
Galati V10	000050.15	+503743.4	EW	0.402	2017–10–16	F5	6396.05	54.35	4.219	0.090	–0.106	0.052	44.76	16.97
ZALD 15	000111.23	+564340.6	EW	0.282618	2014–11–20	F0	6950.06	42.69	3.741	0.070	0.175	0.040	–8.45	6.87
EW Psc	000111.63	+090441.4	EW	0.241202	2016–12–16	G7	5516.42	17.38	4.474	0.025	0.292	0.014	–17.12	3.81
ASASSN-V J000140.29+481741.8	000140.29	+481741.5	EW	0.329783	2017–10–16	G6	5587.83	115.36	4.250	0.190	0.017	0.112	–15.47	8.81
CSS_J000142.2+374956	000142.28	+374956.3	EW	0.359541	2014–12–19	G2	5671.04	311.74	3.962	0.493	–0.596	0.295	–55.37	9.79
GSC 02785–01220	000158.18	+401439.9	EW	0.2787922	2013–11–14	G8	5525.94	24.88	4.193	0.041	0.324	0.023	–25.99	4.74
V0783 And	000205.29	+381322.3	EW	0.2090804	2014–12–19	K7	4207.71	127.41	4.504	0.198	–0.355	0.118	–27.73	7.79
WISE J000222.3+500223	000222.31	+500223.2	EW	0.4410448	2017–10–16	F2	6204.30	41.60	4.100	0.069	0.159	0.040	–69.96	11.57
CSS_J000227.0+433444	000227.01	+433444.9	EW	0.4285856	2014–12–18	A7V	7308.30	121.56	4.277	0.200	–0.363	0.117	–20.31	18.58
ASASSN-V J000322.41+040847.3	000322.42	+040847.0	EW	0.303212	2013–11–21	G8	5520.81	15.84	4.175	0.026	0.300	0.015	10.09	5.23
NSVS 6316462	000327.98	+304715.9	EW	0.38304400	2017–12–14	F9	6004.96	38.82	4.018	0.064	–0.095	0.037	22.78	11.13
NSVS 6316462	000327.99	+304716.1	EW	0.38304400	2012–11–25	F9	5993.17	41.48	3.987	0.068	–0.053	0.040	42.18	11.36
NSVS 6316462	000327.99	+304716.1	EW	0.38304400	2012–11–25	F9	5954.78	36.94	4.020	0.061	–0.077	0.035	27.58	14.79
WISE J000331.6+492356	000331.63	+492356.6	EW	0.3434585	2017–10–16	F6	6048.64	25.41	4.131	0.042	-0.418	0.024	-122.25	12.39
ROTSE1 J000349.50+315316.0	000349.49	+315316.0	EW	0.438080	2012–11–25	F8	6080.90	64.18	3.849	0.106	0.075	0.062	68.35	6.60
V0621 Peg	000414.57	+311508.7	EW	0.39827	2012–11–25	F0	6751.54	312.30	4.147	0.494	–0.441	0.292	–4.22	28.45
WISE J000433.6+453115	000433.67	+453115.7	EW	0.3302411	2017–12–11	K1	5498.42	181.09	4.347	0.293	0.536	0.173	0.52	11.42
ASASSN-V J000438.42+333406.0	000438.40	+333405.9	EW	0.677636	2012–11–25	F0	6862.53	191.81	3.797	0.303	0.034	0.179	–67.58	14.50
NSVS 3641265	000453.32	+391409.8	EW	0.42765025	2013–11–14	F9	5797.84	37.03	4.320	0.061	0.268	0.036	–57.02	8.50
NSVS 3641265	000453.32	+391409.8	EW	0.42765025	2013–11–14	F9	5771.03	71.05	4.270	0.117	0.264	0.069	–45.68	10.83
CSS_J000455.3+395050	000455.36	+395049.9	EW	0.301548	2016–12–27	G3	5333.58	852.34	3.615	—	–0.767	0.790	–39.67	60.70
WISE J000536.5+494201	000536.52	+494201.2	EW	0.5685298	2013–11–22	F0	6836.03	27.99	4.049	0.046	–0.018	0.026	–32.10	14.40
ROTSE1 J000546.47+331545.1	000546.47	+331545.0	EW	0.358822	2012–11–25	F5	6102.96	49.49	4.025	0.081	–0.184	0.048	–11.77	18.39
ROTSE1 J000546.47+331545.1	000546.47	+331545.0	EW	0.358822	2012–11–25	F7	6104.27	78.58	4.104	0.128	–0.144	0.076	–17.69	11.52
ROTSE1 J000604.33+345612.8	000604.33	+345612.7	EW	0.395747	2015–09–25	G0	6015.46	18.48	4.151	0.031	0.012	0.017	–54.09	6.74
ROTSE1 J000604.33+345612.8	000604.33	+345612.8	EW	0.395747	2012–11–30	G0	5974.17	79.20	4.079	0.130	0.075	0.077	–46.65	10.17

Table 2 Catalog of Stellar Atmospheric Parameters for 629 EWs Determined with MRS (the First 30 Observations)

Name (1)	R.A. (2)	Dec. (3)	Type (4)	P (d) (5)	Date (6)	T (K) (7)	E_1 (8)	log(g) (9)	E_2 (10)	[Fe/H] (11)	E_3 (12)	Vr (km s^{-1}) (13)	E_4 (14)
EW Psc	000111.53	+090441.5	EW	0.241202	2018–11–27	5376.50	39.39	3.965	0.045	–0.158	0.028	–7.73	1.43
ASASSN-V J000314.23+103957.3	000314.23	+103957.0	EW	0.356488	2018–11–27	6262.26	24.73	4.554	0.029	0.101	0.018	40.14	1.33
ASASSN-V J000322.41+040847.3	000322.41	+040847.1	EW	0.303212	2018–10–19	5232.38	27.39	3.699	0.031	0.245	0.019	26.91	1.66
ZALD 1	000904.65	+585935.1	EW	0.45218	2018–12–17	5955.22	50.47	4.018	0.063	0.124	0.037	–58.87	1.86
ASASSN-V J002642.20+563436.3	002642.19	+563436.2	EW	0.881697	2018–12–17	8127.42	36.46	4.180	0.044	–0.080	0.026	-166.85	1.25
WISE J003355.3+581603	003355.26	+581604.6	EW|EA	0.9301635	2018–12–17	6015.80	93.90	3.854	0.078	–0.120	0.049	–34.78	1.05
WISE J003355.3+581603	003355.39	+581601.8	EW|EA	0.9301635	2018–12–16	7874.91	47.34	4.103	0.039	–0.059	0.025	19.31	1.05
WISE J003409.3+571224	003409.33	+571224.7	EW	0.7473164	2018–12–17	6716.83	21.47	4.152	0.023	0.321	0.014	–115.68	1.22
CSS_J005223.6+081143	005223.64	+081143.5	EW	0.372762	2017–11–26	6261.07	48.18	4.113	0.061	–0.583	0.037	–71.27	1.54
CSS_J005223.6+081143	005223.64	+081143.5	EW	0.372762	2017–11–28	6261.07	32.17	4.113	0.043	–0.583	0.026	–14.44	2.03
CSS_J005226.7+393537	005226.79	+393536.8	EW	0.44463	2018–10–29	5455.25	45.79	3.097	0.054	–0.610	0.033	–53.69	1.46
CSS_J005251.1+101347	005251.17	+101347.1	EW	0.326842	2018–10–17	5694.57	35.00	3.997	0.041	–0.022	0.025	–27.30	1.84
IY Psc	005414.78	+064109.4	EW	0.401386	2017–11–07	4910.06	30.03	2.289	0.038	–0.994	0.023	–109.35	1.78
IY Psc	005414.78	+064109.4	EW	0.401386	2017–11–26	4910.06	44.64	2.289	0.055	–0.994	0.032	–109.49	1.61
IY Psc	005414.78	+064109.4	EW	0.401386	2017–11–28	4910.06	25.91	2.289	0.033	–0.994	0.020	–100.74	2.09
CSS_J005425.6+081141	005425.61	+081141.2	EW	0.26279	2017–11–07	4811.67	40.86	4.251	0.052	–0.087	0.032	–42.58	1.80
CSS_J005425.6+081141	005425.61	+081141.2	EW	0.26279	2017–11–26	4811.67	89.23	4.251	0.107	–0.087	0.064	–34.38	1.73
CSS_J005425.6+081141	005425.61	+081141.2	EW	0.26279	2017–11–28	4811.67	41.04	4.251	0.052	–0.087	0.032	34.41	3.54
CSS_J005425.6+081141	005425.62	+081141.3	EW	0.26279	2018–10–17	4849.77	34.38	4.293	0.036	–0.110	0.023	–67.49	1.57
V0517 And	005611.68	+354909.9	EW	0.49053	2018–10–29	6505.30	63.54	4.099	0.081	–0.399	0.049	–11.92	1.57
V0518 And	005728.88	+400143.4	EW	0.36115	2018–10–29	6160.22	34.43	4.435	0.040	0.174	0.024	43.08	1.33
CSS_J005735.6+061641	005735.64	+061641.8	EW	0.282878	2017–11–07	4821.83	32.25	3.389	0.042	–1.586	0.025	–6.10	1.77
CSS_J005735.6+061641	005735.64	+061641.8	EW	0.282878	2017–11–26	4821.83	46.51	3.389	0.058	–1.586	0.034	–8.52	1.49
CSS_J005735.6+061641	005735.64	+061641.8	EW	0.282878	2017–11–28	4821.83	21.71	3.389	0.029	–1.586	0.018	–11.30	1.97
CSS_J005820.2+153157	005820.21	+153157.2	EW	0.320254	2018–12–23	5264.93	40.45	3.834	0.051	–0.712	0.031	–45.52	1.59
CSS_J005848.6+160352	005848.58	+160352.7	EW	0.603351	2018–12–23	6496.80	31.59	4.195	0.036	–0.255	0.022	–39.43	0.92
DS Psc	005851.97	+030357.8	EW	0.34249082	2018–10–19	5531.68	103.08	4.374	0.099	0.163	0.064	29.24	1.44
DS Psc	005851.97	+030357.8	EW	0.34249082	2018–10–24	5597.49	15.00	4.160	0.019	0.289	0.011	–1.54	1.36
DS Psc	005851.97	+030357.8	EW	0.34249082	2018–10–28	5597.49	63.28	4.160	0.066	0.289	0.042	–39.29	1.26
DS Psc	005851.97	+030357.8	EW	0.34249082	2018–11–16	5597.49	26.53	4.160	0.032	0.289	0.019	24.84	1.38

In LAMOST DR7 V1.1, stellar atmospheric parameters of 8520 EW-type contact binaries were determined by LRS, while the parameters of 629 ones were procured by medium-resolution spectra (MRS). Those stellar atmospheric parameters include the effective temperature $T_{\rm eff}$, the gravitational acceleration $\log(g)$, metallicity [Fe/H] and radial velocity V_r. They were automatically determined by the LAMOST stellar parameter pipeline when their spectra were regarded as good and reliable (e.g., Wu et al. 2011, 2014; Luo et al. 2015).

To identify EWs and extract data from LAMOST DR7 V1.1, we calculated the distances (in arcsec) between the

Table 3 Mean Stellar Atmospheric Parameters of EWs Observed in LSR (the First 30 Observations)

Name (1)	R.A. (2)	Dec. (3)	P (d) (4)	Times (5)	$\overline{Sp.}$ (6)	$\overline{T_{\rm eff}\,(K)}$ (7)	E_1 (8)	$\overline{\log(g)}$ (9)	E_2 (10)	$\overline{[{\rm Fe/H}]}$ (11)	E_3 (12)
V0467 And	000006.52	+352200.7	0.3535394	1	G6	5650.26	58.84	4.065	0.097	0.405	0.057
V1296 Cas	000024.52	+552748.4	0.3709583	1	G2	6002.19	202.11	4.229	0.314	0.108	0.187
WISE J000025.3+154056	000025.31	+154056.4	0.3283491	1	G2	5853.47	74.64	4.176	0.121	–0.397	0.071
GSC 02781–00387	000030.43	+391107.0	0.2879	1	G7	5584.36	45.12	4.353	0.074	–0.118	0.044
Galati V10	000050.15	+503743.4	0.402	1	F5	6396.05	54.35	4.219	0.090	–0.106	0.052
ZALD 15	000111.23	+564340.6	0.282618	1	F0	6950.06	42.69	3.741	0.070	0.175	0.040
EW Psc	000111.63	+090441.4	0.241202	1	G7	5516.42	17.38	4.474	0.025	0.292	0.014
ASASSN-V J000140.29+481741.8	000140.29	+481741.5	0.329783	1	G6	5587.83	115.36	4.250	0.190	0.017	0.112
CSS _ J000142.2+374956	000142.28	+374956.3	0.359541	1	G2	5671.04	311.74	3.962	0.493	–0.596	0.295
GSC 02785–01220	000158.18	+401439.9	0.2787922	1	G8	5525.94	24.88	4.193	0.041	0.324	0.023
V0783 And	000205.29	+381322.3	0.2090804	1	K7	4207.71	127.41	4.504	0.198	–0.355	0.118
WISE J000222.3+500223	000222.31	+500223.2	0.4410448	1	F2	6204.30	41.60	4.100	0.069	0.159	0.040
CSS _ J000227.0+433444	000227.01	+433444.9	0.4285856	1	A7	7308.30	121.56	4.277	0.200	–0.363	0.117
ASASSN-V J000322.41+040847.3	000322.42	+040847.0	0.303212	1	G8	5520.81	15.84	4.175	0.026	0.300	0.015
NSVS 6316462	000327.98	+304715.9	0.38304400	3	F9	5984.30	26.24	4.008	0.019	–0.075	0.021
WISE J000331.6+492356	000331.63	+492356.6	0.3434585	1	F6	6048.64	25.41	4.131	0.042	–0.418	0.024
ROTSE1 J000349.50+315316.0	000349.49	+315316.0	0.438080	1	F8	6080.90	64.18	3.849	0.106	0.075	0.062
V0621 Peg	000414.57	+311508.7	0.39827	1	F0	6751.54	312.30	4.147	0.494	–0.441	0.292
WISE J000433.6+453115	000433.67	+453115.7	0.3302411	1	K1	5498.42	181.09	4.347	0.293	0.536	0.173
ASASSN-V J000438.42+333406.0	000438.40	+333405.9	0.677636	1	F0	6862.53	191.81	3.797	0.303	0.034	0.179
NSVS 3641265	000453.32	+391409.8	0.42765025	2	F9	5784.43	18.96	4.295	0.035	0.266	0.003
CSS _ J000455.3+395050	000455.36	+395049.9	0.301548	1	G3	5333.58	852.34	3.615	—	–0.767	0.790
WISE J000536.5+494201	000536.52	+494201.2	0.5685298	1	F0	6836.03	27.99	4.049	0.046	–0.018	0.026
ROTSE1 J000546.47+331545.1	000546.47	+331545.0	0.358822	2	F6	6103.61	0.93	4.065	0.056	–0.164	0.028
ROTSE1 J000604.33+345612.8	000604.33	+345612.7	0.395747	2	G0	5994.82	29.20	4.115	0.051	0.043	0.045
WISE J000604.7+474228	000604.77	+474227.9	0.3196552	2	G3	5467.89	123.57	3.593	0.146	–0.524	0.195
ROTSE1 J000613.55+362658.0	000613.54	+362658.0	0.413161	2	F3	6473.34	20.97	4.213	0.022	–0.313	0.006
CSS _ J000642.4+311501	000642.44	+311501.1	0.342065	1	F7	5857.63	112.69	3.943	0.184	–0.614	0.109
UCAC4 457–000142	000646.53	+012151.6	0.272495	1	G9	4962.96	200.41	4.116	0.329	–0.365	0.191
V0687 Peg	000709.61	+262127.8	0.40340	3	F1	6495.51	57.99	4.220	0.039	–0.337	0.090

Table 4 Mean Stellar Atmospheric Parameters of EWs Observed in MRS (the First 30 Observations)

Name (1)	R.A. (2)	Dec. (3)	P (d) (4)	Times (5)	$\overline{T_{\rm eff}\,(K)}$ (6)	E_1 (7)	$\overline{\log(g)}$ (8)	E_2 (9)	$\overline{[{\rm Fe/H}]}$ (10)	E_3 (11)
EW Psc	000111.53	+090441.5	0.241202	1	5376.50	39.39	3.965	0.045	–0.158	0.028
ASASSN-V J000314.23+103957.3	000314.23	+103957.0	0.356488	1	6262.26	24.73	4.554	0.029	0.101	0.018
ASASSN-V J000322.41+040847.3	000322.41	+040847.1	0.303212	1	5232.38	27.39	3.699	0.031	0.245	0.019
ZALD 1	000904.65	+585935.1	0.45218	1	5955.22	50.47	4.018	0.063	0.124	0.037
ASASSN-V J002642.20+563436.3	002642.19	+563436.2	0.881697	1	8127.42	36.46	4.180	0.044	–0.080	0.026
WISE J003355.3+581603	003355.26	+581604.6	0.9301635	1	6015.80	93.90	3.854	0.078	–0.120	0.049
WISE J003355.3+581603	003355.39	+581601.8	0.9301635	1	7874.91	47.34	4.103	0.039	–0.059	0.025
WISE J003409.3+571224	003409.33	+571224.7	0.7473164	1	6716.83	21.47	4.152	0.023	0.321	0.014
CSS _ J005223.6+081143	005223.64	+081143.5	0.372762	2	6261.07	0.00	4.113	0.000	–0.583	0.000
CSS _ J005226.7+393537	005226.79	+393536.8	0.44463	1	5455.25	45.79	3.097	0.054	–0.610	0.033
CSS _ J005251.1+101347	005251.17	+101347.1	0.326842	1	5694.57	35.00	3.997	0.041	–0.022	0.025
IY Psc	005414.78	+064109.4	0.401386	3	4910.06	0.00	2.289	0.000	–0.994	0.000
CSS _ J005425.6+081141	005425.61	+081141.2	0.26279	4	4821.19	19.05	4.261	0.021	–0.093	0.012
V0517 And	005611.68	+354909.9	0.49053	1	6505.30	63.54	4.099	0.081	–0.399	0.049
V0518 And	005728.88	+400143.4	0.36115	1	6160.22	34.43	4.435	0.040	0.174	0.024
CSS _ J005735.6+061641	005735.64	+061641.8	0.282878	3	4821.83	0.00	3.389	0.000	–1.586	0.000
CSS _ J005820.2+153157	005820.21	+153157.2	0.320254	1	5264.93	40.45	3.834	0.051	–0.712	0.031
CSS _ J005848.6+160352	005848.58	+160352.7	0.603351	1	6496.80	31.59	4.195	0.036	–0.255	0.022
DS Psc	005851.97	+030357.8	0.34249082	8	5579.25	33.99	4.211	0.094	0.236	0.107
ASAS J005904+0551.6	005903.96	+055132.9	0.272792	7	5729.36	145.43	4.570	0.038	–0.142	0.237
VSX J005935.2+174707	005935.25	+174707.3	0.249131	1	4468.75	57.51	4.392	0.066	0.045	0.040
1SWASP J010056.53+352541.4	010056.58	+352541.5	0.333809	1	5417.44	22.76	4.221	0.023	0.318	0.015
NSVS 3802179	010205.99	+395237.6	0.50698	1	6748.41	26.10	4.300	0.027	–0.294	0.017
ASAS J010322+0230.7	010321.83	+023040.6	0.28485016	9	5078.04	38.44	3.762	0.060	–0.594	0.068
CSS _ J011046.2+020115	011046.19	+020115.0	0.29219	1	6135.40	36.36	4.893	0.043	–0.065	0.026
WISE J011047.1+564049	011047.18	+564049.1	0.3860844	1	6838.52	36.46	4.645	0.044	0.188	0.026
T-And0-04813	011638.93	+473316.2	0.5524805	1	6040.51	62.11	4.185	0.083	0.117	0.051
2MASS J01175869+5651101	011758.70	+565110.2	0.423953	1	6018.10	5.56	4.322	0.007	–0.251	0.005
CSS _ J012221.7+023832	012221.67	+023833.0	0.332129	1	6145.68	44.68	4.441	0.055	0.129	0.032
WISE J012325.3+585752	012325.39	+585752.5	0.6449933	1	7969.47	35.51	4.013	0.043	–0.187	0.026

two positions determined by the coordinates given in VSX and by LAMOST. Based on the same criterion Dist$<$ 2 arcsec applied by Qian et al. (2017), those EWs were identified from the LAMOST samples. Stellar atmospheric parameters of the 8520 EWs determined with LRS are catalogd in the order of their coordinates. When they were observed two or more times on different dates, we list all of the parameters. Those displayed in Table 1 are the first 30 lines of the observations. The whole catalog is available through the internet (the electronic version of the catalog is at the website[2]). The first five columns in the table include binary names, their right ascensions (RA) and declinations (DEC), types of light variation and orbital periods that are from the VSX catalog. Those shown in column (6) are the distances that were used to identify those EWs from the LAMOST samples based on the criterion Dist< 2 arcsec. The observing dates are listed in column (6), while the determined spectral types of those EWs are provided in column (8). The stellar atmospheric parameters, $T_{\rm eff}$, $\log(g)$, [Fe/H] and V_r of the 8520 EWs, are listed in columns (8), (10), (12) and (14) respectively. E_1, E_2, E_3 and E_4 in the table are their errors respectively. The MRS parameters of the 629 EWs are also cataloged and those shown in Table 2 are the first 30 lines. The whole catalog is available at the website[3]. The arrangement in Table 2 is the same as that in Table 1. The only difference is no spectral types were determined from medium-resolution stellar spectra.

To utilize the stellar atmospheric parameters of those EWs more conveniently, when they were observed two or more times, their effective temperature $T_{\rm eff}$, the gravitational acceleration $\log(g)$ and metallicity [Fe/H] were averaged. For each target, the stellar parameters are the weighted mean values of all their observations at different times. The weight for each data point is the inverse square of its error. The final error of the mean parameter is derived with the standard error transfer formula by assuming that each observation is independent from the other. As for the radial velocity V_r, we did not average them because they were observed at different phases and are varying with time. We also cataloged the averaged parameters at the websites [45]. Those displayed in Tables 3 and 4 are the first 30 lines of the catalogs. The explanations of those columns in Tables 3 and 4 are the same as the corresponding ones in Tables 1 and 2. The observational times are provided in column (5).

Among the 8520 EWs observed by LRS, the orbital periods of 8510 samples are given in VSX. The relative distribution (the ratio of the number to the whole sample) of the orbital period for the 8510 EWs is displayed in Figure 2 as red dots. Also displayed in the figure is the relative period distribution of all EWs in VSX whose orbital periods are known (blue dots). For comparison, the distribution of 628 EWs observed by MRS (only one has no period) is also depicted in the figure (green dots). As visible in the figure, the LRS distribution and the all-EW distribution nearly overlap. This suggests that the LRS EWs could be utilized to represent the properties of all the EWs in the whole VSX catalog. However, the distribution of EWs observed by MRS shows a little larger deviation from the other two when the periods are shorter than 0.35 d. This is caused by the fact that short-period EWs are usually faint and the number of observed faint targets is smaller than that of bright ones by MRS. This property could be seen directly from Figure 3 where the correlation between the effective temperature and metallicity [Fe/H] is displayed. When the temperatures of EWs are lower than 4700 K, few of them were observed by MRS. These cool EW-type contact binaries usually have lower metallicity, indicating that they may be old systems. They are formed over long times through AML via magnetic braking (Qian et al. 2017).

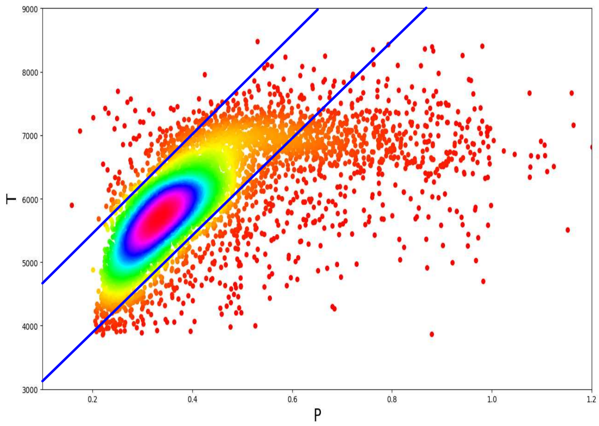

Fig. 4 Heat map of the correlation between orbital period and effective temperature based on parameters of 8510 contact binaries observed by LRS. Most EWs are located in the two blue lines that are the boundaries of normal EWs. Systems near the right border are marginal contact systems, while those close to the left border are deep contact ones.

3 MARGINAL CONTACT BINARY SYSTEMS AND THEIR PROGENITORS

As aforementioned, since the relative period distribution of EWs observed by LRS is the same as that of all EWs in VSX, they can be used to investigate the properties of all the EWs. For contact binaries, there is a famous relation called period-color (or temperature) relation (Eggen 1967; Rucinski 1998). To investigate this relation in detail by utilizing LAMOST stellar atmospheric parameters, the heat map for this relation is exhibited in Figure 4. As plotted in the figure, most EWs are located within the two blue lines. Their descriptions are as follows

$$\begin{aligned} T &= 4000 + 7500 \times P \\ T &= 2450 + 7500 \times P. \end{aligned} \tag{1}$$

They are the boundaries of normal EWs. Systems near the right boundary usually have longer orbital period for a giv-

[2] http://search.vbscn.com/2020EW.table1.txt
[3] http://search.vbscn.com/2020EW.table2.txt
[4] http://search.vbscn.com/2020EW.table3.txt
[5] http://search.vbscn.com/2020EW.table4.txt

Table 5 Parameters of Pre-Contact Binaries

Star	Period (d)	dP/dt (10^{-7}d yr^{-1})	$q(M_2/M_1)$	T_1 (K)	T_2 (K)	M_1 ($M_\odot$)	M_2 ($M_\odot$)	R_1 ($R_\odot$)	R_2 ($R_\odot$)	Ref
V361 Lyr	0.30961	–0.84	0.694	6200	4500	1.26	0.87	1.02	0.72	(1) (2)
V369 Cep	0.32819	–0.73	0.85	5348	4985	0.78	0.66	0.89	0.70	(3)
V473 Cas	0.41546	–0.76	0.493	5830	4378	1	0.48	1.19	0.83	(4)
GR Tau	0.42985	–0.42	0.2192	7500	3434	1.45	0.32	1.49	0.71	(5) (6)
CN And	0.46279	–1.4	0.3885	6500	5922	1.299	0.505	1.425	0.91	(7) (8)
FT Lup	0.47008	–1.85	0.465	6700	3916	1.43	0.61	1.43	0.94	(9)
BS Vul	0.47597	–0.24	0.34	7000	4632	1.52	0.52	1.54	0.93	(10)
TT Cet	0.48595	–0.501	0.43	7091	5414	1.57	0.68	1.55	1.04	(11)
RT Scl	0.51156	–1.29	0.433	7000	4820	1.63	0.7	1.59	1.10	(12) (13)
V1010 Oph	0.66144	–3.97	0.47	7500	5132	1.887	0.887	2.01	1.40	(14) (15)
BL And	0.72238	–0.24	0.377	7500	4830	1.8	0.7	2.13	1.35	(16)
V388 Cyg	0.85905	–4.11	0.3653	8750	5543	2.08	0.79	2.52	1.54	(17) (18)
TT Her	0.9121	–1.82	0.439	7239	4690	1.56	0.68	2.3	1.49	(19) (20)

Ref: (1) Lister (2009); (2) Hilditch et al. (1997); (3) Zhu et al. (2014); (4) Zhu et al. (2009); (5) Qian (2002); (6) Gu et al. (2004); (7) Van Hamme et al. (2001); (8) Cai et al. (2019); (9) Lipari & Sistero (1986); (10) Zhu et al. (2012); (11) Tian & Chang (2020); (12) Duerbeck & Karimie (1979); (13) Hilditch & King (1986); (14) Lipari & Sistero (1987); (15) Siwak et al. (2010); (16) Zhu & Qian (2006); (17) Kang et al. (2001); (18) Oh et al. (1997); (19) Milano et al. (1989); (20) Terrell & Nelson (2014)

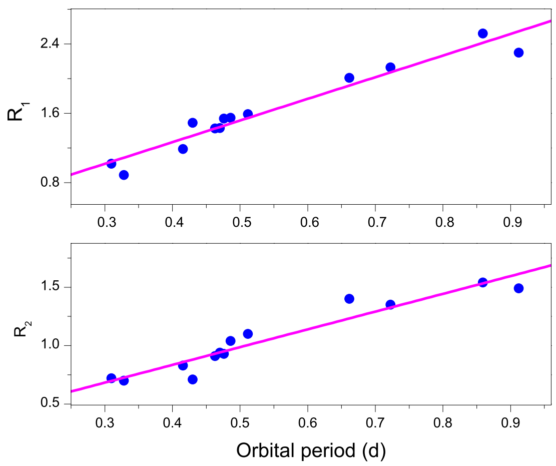

Fig. 5 Relations between orbital period and radius of the primary component (*upper panel*) and radius of the secondary component (*lower panel*). Data come from Table 5. The magenta lines signify linear fits.

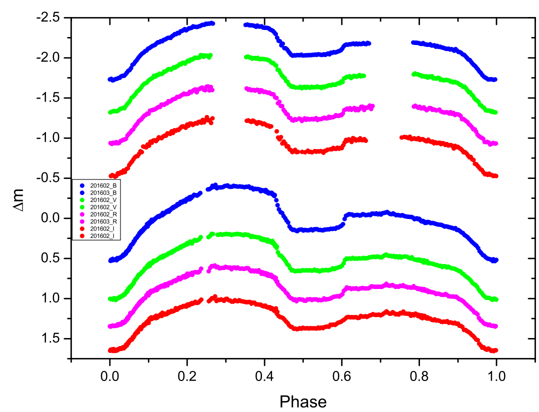

Fig. 6 Two sets of $BVRI$ light curves for the V361 Lyr-type semi-detached binary UV Mon obtained in February and March, 2016 by utilizing the 1.0-m telescope administered by Yunnan Observatories.

en temperature. They have higher orbital angular momentum and usually have marginal (or shallow) contact configuration with fill-out factor less than 20%. By comparing stellar parameters of EWs with EAs, Qian et al. (2017, 2018) found that some EWs had evolved from EAs that underwent case A mass transfer and AML via magnetic braking. Those marginal contact systems are believed to be newly-formed contact binaries and are at the beginning of their contact phase.

The original EA-type detached binaries are thought to be the progenitors of W UMa contact binaries. They are generally low mass and magnetically active stars. As a result of the evolutionary expansion of the primary component together with AML caused by magnetic braking, the short-period detached progenitors will evolve to contact binaries through the near contact binary (NCB) phase (Guinan & Bradstreet 1988; Stępień & Kiraga 2013; Qian et al. 2018). NCBs have been defined as a kind of close binaries with both components filling or nearly filling their critical RLs. Among them, one subtype has significant observational evidence of mass transfer which is thought to be the pre-contact binary. They are the semi-detached binaries with a lobe-filling primary. Under primary-to-secondary mass transfer, their orbital periods are decreasing. Their light curves show stable enhanced luminosity around the left shoulder of the secondary minimum due to the stream of mass heating the facing hemisphere of the secondary component (Zhu et al. 2009; Tian & Chang 2020). Stars pass through this pre-contact stage relatively quickly, which makes them quite rare. We collected some confirmed cases which have absolute parameters and period decrease rates. They are list-

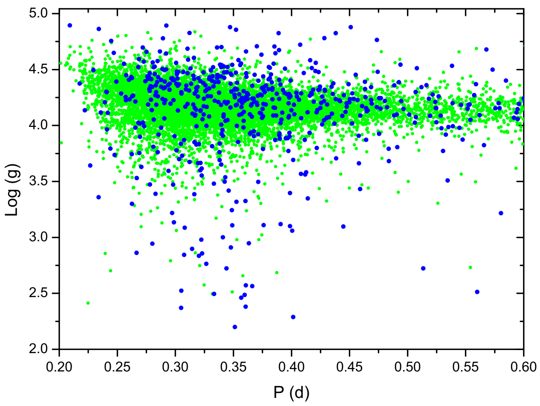

Fig. 7 The relation between orbital period (P) and the gravitational acceleration $\log(g)$ for EWs with $P < 0.6$ d. Symbols are the same as those in Fig. 3.

ed in Table 5. The period and radius of these pre-contact binaries follow a good linear relationship, see Figure 5. This implies that their components are very close to their own RLs, which is in agreement with their near-contact configuration. Among them, a special case is the V361 Lyr system (Richter & Andronov 1986; Kaluzny 1990; Hilditch et al. 1997). It has an extremely asymmetric light curve, which makes it the best target to study mass transfer. For more than 20 years, V361 Lyr was identified as a unique case. Recently, two new V361 Lyr-type stars have been reported, VSX J052807.9+725606 (Virnina 2013) and HAT 141-03513 (Wolf & Kučáková 2020). Here we report the fourth one discovered by us, UV Mon. Its multi-wavelength light curves observed in 2016 are plotted in Figure 6. They are primary filling semi-detached NCBs with a rather large steady hot region caused by the accretion stream. In order to test the theory, more such pre-contact binaries are needed. Thanks to large sky surveys, such as Kepler, TESS, Gaia and LAMOST, a large number of spectra and high-quality continuous photometric observations of binaries can be obtained, which will be helpful for searching for them.

As the period decreases, the pre-contact binaries will evolve to marginal contact systems and are located near the right boundary of the period-temperature relation in Figure 4. They have relatively larger mass ratios. According to the predictions of the theory of TRO (e.g., Lucy 1976; Flannery 1976; Robertson & Eggleton 1977), contact binaries must undergo oscillations around the state of marginal contact. Each oscillation comprises a shallow contact phase followed by a semi-detached phase. During the shallow contact phase, the orbital periods should increase because of conservative mass transfer from the less massive component to the more massive one. However, many shallow contact binaries have been detected with decreasing periods (Qian et al. 2013). To interpret both increases and decreases in the orbital periods of contact binaries, an evolutionary scenario was proposed by Qian (2001a,b, 2003) in which contact binary stars are undergoing TRO with a variable AML via a change in the degree of contact, i.e., the higher the degree of contact is, the lower the rate of AML would be. This evolutionary scheme predicts that contact binaries are oscillating around a critical mass ratio (Qian 2001a, 2003). However, we did not know on what physical conditions the direction of mass transfer should be changed. Mass transfer makes the evolution of binaries be different from that of single stars. Compared with other types of close binaries, mass transfer in contact systems is more complicated. Via a CE, matter can be free to transfer between the two components. No models could predict mass transfer with varying directions.

As featured in Figure 4, some cool marginal short-period contact binaries are composed of late type components with temperatures below 5000 K and orbital periods shorter than 0.25 d. Compared with other long-period EWs, their metallicities are lower (see Fig. 3), while their the gravitational accelerations are higher (see Fig. 7). These properties indicate that their component stars have nearly not evolved and they may be older population systems. As pointed out by Qian et al. (2017, 2018), these systems may be formed from short-period cool EAs through AML via magnetic braking with little mass transfer. A good example is the short-period Siamese twin BI Vul, which is a marginal contact binary ($f = 8.7\%$) that contains two very similar cool components ($q = 1.037$) (Qian et al. 2013). The formation and evolution of the system are mainly driven by AML via magnetic braking because their main-sequence evolutionary times are much longer than the age of the Galaxy.

Other main characteristics of marginal contact binaries (actually for all EWs) are the A- and W-subtype phenomena. Binnendijk (1970) defined two subtypes (A- and W-subtype) of contact binaries according to their light curves. For A-subtype binaries, the more massive components are hotter than the less massive components, while W-subtype binaries are the opposite. Lucy (1973) and Mochnacki & Whelan (1973) firstly proposed that the thickness of a CE will cause the two subtypes to exhibit different light curves. They thought the W-subtype binaries should have shallow CEs, while A-subtypes have low mass ratios. However, this view was then in trouble (for details see Zhang et al. 2020b). Later on, this issue was debated from different aspects, such as mean density, angular momentum, mass and energy transfer by some authors (e.g., Mochnacki 1981; Hilditch, King & McHilditch et al. 1988; Gazeas & Niarchos 2006; Gazeas & Stępień Gazeas & Stępień (2008)), but an agreement has not been reached yet. Primaries of contact binaries are on the main sequence just like components of detached binaries (e.g., Lucy 1968b; Mochnacki 1981; Rucinski 1985; Eggleton 2006), but secondary components manifest an excess in radius and luminosity (e.g., Yakut & Eggleton 2005; Yildiz & Doğan (2013)). Based on these two special properties, Zhang et al. (2020b) thought that the two subtypes of contact binaries came from different evolutionary pathways. Overluminosity in A-subtype is caused by the reason that the secondaries have evolved from more massive initial stars, while W-subtype is due to energy transfer. In addition, they thought the W-subtype contact binaries have experienced one or several TRO cycles. As mentioned above, energy transfer plays a very important role in evolution of W-subtype binaries. However, the driving mechanism of energy transfer is still unknown. Also, whether the two subtypes have some evolutionary relationship or there is no relation between these two subtypes are still open questions. In the future, more systematic observational studies of these two subtypes are needed.

The structure and detailed evolutionary process during the contact phase are still open questions, but there is no doubt that the whole lifetime of a contact binary is accompanied byAML. The orbital angular momentum of a binary system could be written as the following

$$J_{orb} = \frac{G^{1/12}}{(4\pi^2)^{1/6}} \frac{q}{(1+q)^2} M_t^{1/4} P^{1/3}, \tag{2}$$

where G is the gravitational constant, and P and q are the orbital period and mass ratio, respectively. For a given total binary mass M_t, the orbital angular momentum J_{orb} depends mainly on the orbital period and mass ratio. It will decrease with the decreases of period and mass ratio. Therefore, the marginal systems will evolve into deep contact binaries with lower mass ratios.

4 DEEP AND LOW-MASS RATIO CONTACT BINARY SYSTEMS

DLMCB systems have shorter orbital periods and lower mass ratios. Equation (3) tells us they posses the lowest angular momentum among contact binaries and they are at the end evolutionary stage of tidally-locked magnetic-wind driven evolution. Qian et al. (2005a, 2006b) suggested that if a contact binary has mass ratio $q \leq 0.25$ and fill-out factor $f \geq 50\%$, it can be called a DLMCB. Such a contact binary is the progenitor of a merger owing to the dynamical evolution (Li et al. 2008). The mergers could be some fast-

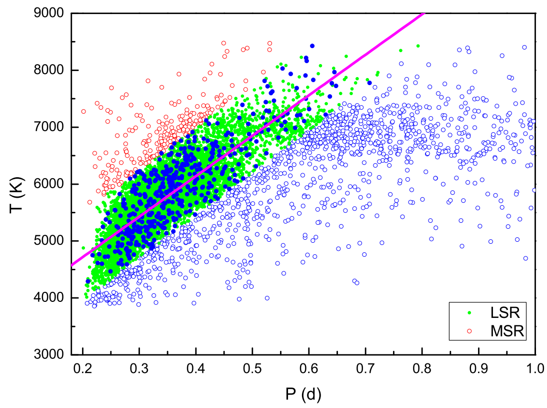

Fig. 8 Correlation between the orbital period and effective temperature based on normal EWs observed by LRS and MRS (*green and blue dots* respectively). Red open circles refer to binaries located above the left boundary of normal EWs, while blue open circles to systems below the right boundary. Systems near the left border are deep contact binaries.

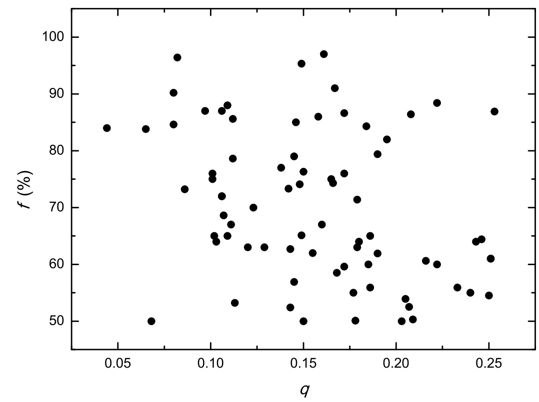

Fig. 9 The relation between mass ratio and fill-out factor for DLMCBs.

rotating single stars like FK Com-type stars, or could be blue stragglers (BSs).

The correlation between orbital period and effective temperature based on all normal EWs is shown in Figure 7 where green dots refer to contact binaries observed in LRS, while blue dots to those systems observed in MRS. Based on data from normal EWs, a least-squares solution yields the following equation

$$T = 3294(\pm 17) + 7112(\pm 47) \times P. \tag{3}$$

The orbital period of contact binaries can be determined more easily. This relation could be applied to estimate the temperature of the primary component. For example, a typical contact binary with a period of 0.31 d has a primary

Table 6 Parameters of Deep and Low-mass Ratio Contact Binaries

Star	Period (d)	q_{ph}	dP/dt ($\times 10^{-7}$ d yr^{-1})	f (%)	i (°)	T_1 (K)	T_2 (K)	Reference
V1187 Her	0.3107	0.044	-1.5	84.0	66.0	6250	6682	Caton et al. (2019)
V857 Her	0.3822	0.065	$+2.90$	83.8	85.3	8300	8513	Qian et al. (2005b); Qian & Yang (2005)
ASAS J083241+2332.4	0.3113	0.068	$+8.85$	50.0	82.7	6300	6667	Sriram et al. (2016)
AW UMa	0.4387	0.080	-2.03	84.6	78.3	7175	7022	Yang (2008); Rucinski (2015)
ZZ Psc	0.3739	0.080		76.2	90.7	6510	6426	Wadhwa (2006)
V870 Ara	0.3997	0.082		96.4	70.0	5860	6210	Szalai et al. (2007)
KIC 5374883	0.4197	0.086		73.2	66.5	5800	5683	Li & Liu (2020b)
KIC 11097678	0.9997	0.097		87.0	85.1	6493	6426	Zola et al. (2017)
AW CrB	0.3609	0.101	$+3.58$	75.0	82.1	6700	6808	Broens (2013)
KIC 10007533	0.6481	0.101		76.0	90.0	6810	6356	Zola et al. (2017)
KIC 8145477	0.5658	0.102		65.0	90.0	6800	6496	Zola et al. (2017)
DN Boo	0.4476	0.103		64.0	60.0	6095	6071	Şenavcı et al. (2008)
J082243+1927	0.2800	0.106		72.0	75.6	5960	6078	Kandulapati et al. (2015)
ASAS J082243+1927.0	0.2801	0.106		72.0	76.6	5960	6078	Kandulapati et al. (2015)
KIC 9350889	0.7259	0.106		87.0	79.9	6725	6749	Zola et al. (2017)
V1191 Cyg	0.3134	0.107	$+4.50$	68.6	80.4	6500	6626	Zhu et al. (2011)
CK Boo	0.3552	0.109	$+0.98$	65.0	64.9	6200	6291	Rucinski & Lu (1999); Yang et al. (2012)
KIC 3127873	0.6715	0.109		88.0	90.0	6070	5702	Zola et al. (2017)
KIC 8804824	0.4574	0.111		67.0	90.0	7200	6733	Zola et al. (2017)
FG Hya	0.3278	0.112	-1.96	85.6	82.3	5900	6012	Lu & Rucinski (1999)
GR Vir	0.3278	0.112	-4.32	78.6	83.4	6300	6163	Rucinski & Lu (1999); Qian & Yang (2004)
V1222 Tau	0.2954	0.112	$+81.9$	85.6	82.3	5900	6012	Liu et al. (2015)
AL Lep	0.4486	0.120		62.7	73.8	6008	5907	Wadhwa (2005)
KIC 7698650	0.5992	0.123		70.0	85.4	6110	6082	Zola et al. (2017)
ϵ CrA	0.5914	0.129		63.0		6700		Shobbrook & Zola (2006)
V776 Cas	0.4404	0.138	-11.7	77.0	52.9	6700	6725	Zola et al. (2004) ; Zhou et al. (2016)
V345 Gem	0.2748	0.142	$+0.59$	73.3	72.9	6115	6365	Yang et al. (2009)
V410 Aur	0.3664	0.143	$+8.22$	52.4	78.6	6040	5915	Yang et al. (2005); Rucinski et al. (2003)
V710 Mon	0.4052	0.143	$+1.95$	62.7	79.9	6145	6294	Liu et al. (2014)
DZ Psc	0.3661	0.145	$+4.33$	79.0	80.5	6210	6287	Yang et al. (2013)
HV Aqr	0.3734	0.145	-0.88	56.9	79.2	6460	6669	Li & Qian (2013)
KIC 9776718	0.5444	0.146		85.0	77.2	6500	7019	Li et al. (2020)
XY LMi	0.4369	0.148	-1.67	74.1	81.0	6144	6093	Qian et al. (2011)
EM Psc	0.3440	0.149	$+39.7$	95.3	88.6	5300	4987	Qian et al. (2008b)
V416 Gem	0.2563	0.149		65.1	73.2	5420	5420	Kjurkchieva et al. (2017)
ASAS J113031–0101.9	0.2710	0.150		50.0	88.0			Pribulla et al. (2009a)
TYC 4157–0683–1	0.3961	0.150		76.3	79.7	6037	5888	Acerbi et al. (2014)
KIC 9453192	0.7188	0.155		62.0	89.5	6730	6239	Zola et al. (2017)
KIC 8539720	0.7450	0.158		86.0	85.1	6350	6119	Zola et al. (2017)
KIC 12055014	0.4999	0.160		67.0	90.0	6456	6439	Zola et al. (2017)
KIC 11144556	0.6430	0.161		97.0	76.8	6428	6318	Zola et al. (2017)
AH Aur	0.4941	0.165	-2.75	75.0	76.1	6200	6418	Gazeas et al. (2005); Rucinski & Lu (1999)
TV Mus	0.4457	0.166	-2.16	74.3	77.2	5980	5808	Qian et al. (2005a)
KIC 3104113	0.8468	0.167		91.0	79.1	5910	5994	Zola et al. (2017)
AH Cnc	0.3604	0.168	$+4.29$	58.5	90.0	6300	6265	Qian et al. (2006a)
TYC 1337–1137–1	0.4755	0.172	$+10.1$	76.0	81.0	6400	6245	Liao et al. (2017)
AS ArB	0.3807	0.172	$+3.46$	59.6	78.4	6550	6498	Liu et al. (2017)
II UMa	0.8252	0.172	$+4.88$	86.6	77.8	6550	6554	Zhou et al. (2016)
KIC 8496820	0.4370	0.177		55.0	82.5	6300	6593	Li & Liu (2020a)
CU Tau	0.4125	0.178	-18.1	50.1	74.0	5900	5938	Qian et al. (2005a)
CSS J075258	0.4299	0.179		63.0	84.3	6094	6227	Kjurkchieva et al. (2017)
V728 Her	0.4713	0.179	$+1.92$	71.4	68.7	6622	6794	Nelson et al. (1995)
Y Sex	0.4198	0.180		64.0	76.1	6210	6093	McLean & Hilditch (1983); Yang & Liu (2003)
TY Pup	0.8192	0.184	$+0.557$	84.3	83.6	6900	6915	Sarotsakulchai et al. (2018)
IK Per	0.6760	0.185	-2.59	60.0	78.1	9070	8300	Zhu et al. (2005)
V2388 Oph	0.8023	0.186		65.0	76.6	6900	6505	Rucinski et al. (2002); Yakut et al. (2004)
XY Boo	0.3706	0.186	$+6.25$	55.9	69.0	6324	6307	Yang et al. (2005); McMcLean & Hilditch (1983)
HV UMa	0.7108	0.190		61.9	57.3	7300	7000	Csák et al. (2000)
TYC 3836-0854-1	0.4156	0.190	$+11.1$	79.4	77.5	6332	6292	Liao et al. (2017)
MQ UMa	0.4760	0.195		82.0	65.6	6352	6224	Zhou et al. (2015)
V1853 Ori	0.3830	0.203		50.0	83.2	6200	6261	Samec et al. (2011)011)
DN Aur	0.6169	0.205		53.9	76.9	6830	6750	Goderya et al. (1996)
TZ Boo	0.2972	0.207	-0.21	52.5	85.5	5890	5873	Pribulla et al. (2009b); Christopoulou et al. (2011)
NSVS 6859986	0.3836	0.208		86.4	89.0	5100	5100	Kjurkchieva et al. (2019)
BO Ari	0.3182	0.209	-3.49	50.3	85.7	5920	6055	Gürol et al. (2015)
V409 Hya	0.4723	0.216	$+5.41$	60.6	89.5	7000	6730	Na et al. (2014)

Table 6 *Continued.*

Star	Period (d)	$q_{\rm ph}$	dP/dt ($\times 10^{-7}$ d yr^{-1})	f (%)	i (°)	T_1 (K)	T_2 (K)	Reference
FN Cam	0.6771	0.222	+4.38	88.4	71.2	6700	6848	Pribulla et al. (2002); Hu et al. (2018)
MW Pav	0.7950	0.222	+0.006	60.0	86.4	6900	6969	Alvarez et al. (2015)
QX And	0.4122	0.233	+2.48	55.9	56.2	6500	6217	Qian et al. (2007a); Milone et al. (1995)
KIC 10267044	0.4300	0.240		55.0	89.6	6808	6700	Zola et al. (2017)
YY CrB	0.3766	0.243	−6.727	63.4	77.0	6135	6142	Essam et al. (2010); Yu et al. (2015)
AP Aur	0.5694	0.246	+8.14	64.4	75.9	9016	8703	Li et al. (2001)
KN Per	0.8665	0.250	+4.18	54.5	83.6	7650	7288	Goderya et al. (1997)
BU Vel	0.5163	0.251		61.0	84.9	7500	7448	Twigg (1979)
V407 Peg	0.6369	0.251		61.0	87.6	6980	6484	Lee et al. (2014)
V343 Ori	0.8091	0.253	+4.32	86.9	79.7	7150	7312	Yang (2009)

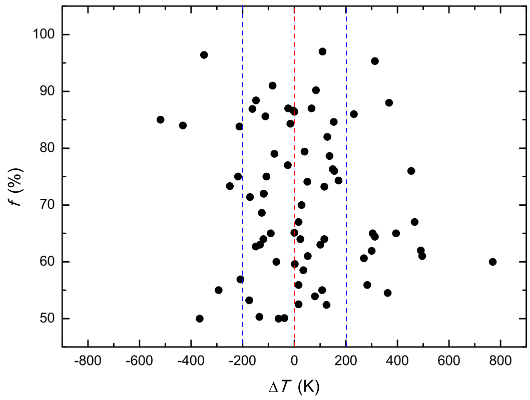

Fig. 10 The relation between temperature difference and contact degree for DLMCBs. $\Delta T = T_1 - T_2$. The dashed red line signifies that the temperature of the primary component is equal to the temperature of the secondary component, implying a complete and efficient energy transfer. The systems to the right of the dashed red line should be A-subtype contact binaries, while the others should be W-subtype systems. As a system with good energy transfer, it should be located between the two blue dashed lines.

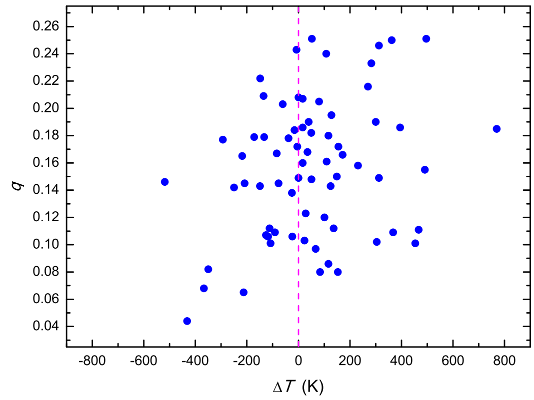

Fig. 11 The relation of the temperature difference to the mass ratio for DLMCBs. As displayed in Fig. 10, the dashed red line signifies that the temperature of the primary component is equal to the temperature of the secondary component. The temperature difference is weakly correlated with the mass ratio.

temperature of about 5500 K. As we can see in Figure 8, for a given temperature, normal systems near the left boundary have shorter orbital periods and they are usually deep contact systems. Therefore, the LAMOST data are very useful for selecting targets for detailed follow-up observation and investigation, and more and more DLMCBs will be detected in the future. Objects (red open circles in Fig. 7) located above the left boundary of normal EWs may be (i) pulsating stars that are misclassified as EWs or (ii) EWs containing hotter third bodies. They need further observations and studies.

The condition of merging for a binary is that the orbital angular momentum is less than three times the rotational angular momentum. Because of the orbital constraint by the contact configuration, a contact binary with a lower mass ratio is closer to that condition. This could be observed as the minimum mass ratio of contact binaries. On the other hand, deep contact indicates a thick CE, which is also unstable. Dual instabilities cause the DLMCBs to have a high possibility of merger. In fact, the progenitor of the observed merger V1309 Sco should be a DLMCB (Zhu et al. 2016). Moreover, the merger of V1309 Sco is now observed as a BS (Ferreira et al. 2019).

The systematic study of DLMCBs was started in 2004 (Qian & Yang 2004). During the last sixteen years, many DLMCBs were detected and studied. Yang & Qian (2015) collected 46 DLMCBs and demonstrated some statistical relationships among the parameters. In this review, 76 DLMCBs were collected and are listed in Table 6. The relation between the mass ratio and fill-out factor is displayed in Figure 9. As demonstrated in the figure, no expected parabolic relation is observed, indicating that those relationships need further investigation.

The common convective envelope (CCE) was thought to be an efficient path for energy transfer from the primary component to the secondary component. Thick CCE should be more efficient for energy transfer than thin CCE.

The temperature difference could be an indicator of efficiency for energy transfer. From this point of view, the CCEs of DLMCBs are very thick and they should have a small temperature difference between the two components (e.g., $\Delta T = T_1 - T_2 < 300\,\mathrm{K}$). However, we do not see this trend in Figure 10. For some DLMCBs, the absolute temperature differences are larger than 500 K. The relation between the temperature difference and the mass ratio for DLMCBs is plotted in Figure 11. As displayed in the figure, there is a weak correlation between the two parameters. Low-mass ratio systems usually have lower temperature difference, indicating that the small secondary components have a higher temperature than the very massive primary. This is hard to understand if they are normal main-sequence stars.

At the end of the section, we focus on some DLMCBs with extremely low mass ratio such as SX Crv ($q = 0.066$, Rucinski et al. 2001), V857 Her ($q = 0.065$, Qian et al. 2005b), ASAS J083241+2332.4 ($q = 0.068$, Sriram et al. 2016) and V1187 Her ($q = 0.044$, Caton et al. 2019). These contact binaries all have extreme mass ratios lower than the theoretically predicted value. Until now, the minimum mass ratio has remained an open question. We think only constant observation can gradually resolve this mystery. When the orbital angular momentum of a binary system is smaller than three times the spin angular momentum, due to tidal instability, the binary will merge into a single, rapidly rotating star (Hut 1980). Based on this, Rasio (1995) and Arbutina (2007, 2009) studied the minimum mass ratio of contact binaries theoretically. However, we notice that their result depends a lot on the dimensionless gyration radii of primary components (k_1). However, k_1 is hard to determine, even impossible. Since a different stellar structure may produce a different value of k_1 (Jiang et al. 2010), and if one considers the differential rotation of a star, the situation is more complicated (Yakut & Eggleton 2005; Li & Zhang 2006).

New high-resolution spectroscopic observations on the well-known DLMCB system AW UMa reveal that it is a semi-detached binary together with vigorous mass motions present in the system (Pribulla & Rucinski 2008; Rucinski 2015). A "pedestal" of large rotational/orbital velocities was found around the primary that is covered with very slowly drifting spots and a dense network of ripples. All of these complex structures cannot be explained. It is possible that it is a group of unusual systems in which the secondary is in an advanced evolutionary stage with hydrogen depleted in its core as predicted by Stępień (2009).

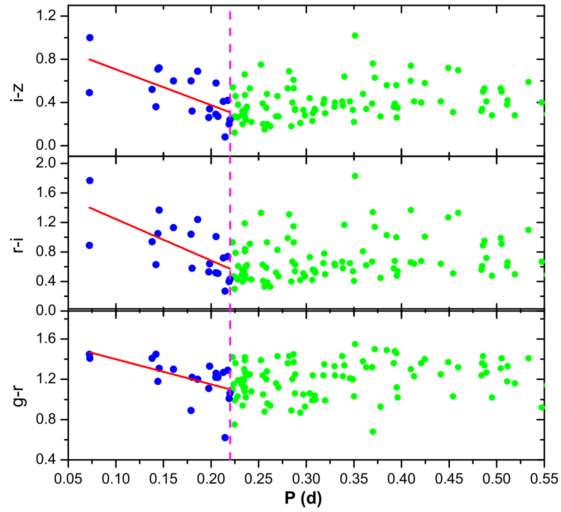

Fig. 12 Color-period relations for M-type binary stars. Green dots refer to binary systems with orbital periods longer than 0.22 d, while blue ones to those with periods shorter than 0.22 d. The dashed magenta line is the boundary. It is apparent that the colors are correlated with the period when orbital period is shorter than 0.22 d.

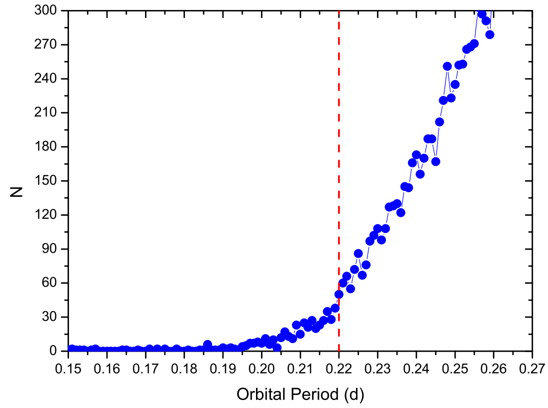

Fig. 13 Period distribution of short-period contact binaries with orbital period shorter than 0.26 d. The red dashed line represents the old short-period limit of contact binaries.

5 CONTACT BINARY SYSTEMS NEAR AND BELOW THE SHORT-PERIOD LIMIT

The period distribution for short-period contact binaries was investigated by some researchers (e.g., Rucinski 1992, 2007; Becker et al. 2011; Norton et al. 2011; Nefs et al. 2012; Drake et al. 2014). It has been suspected that there is a short-period limit for contact binaries at about 0.22 d (e.g., Rucinski 1992, 2007). Norton et al. (2011) presented light curves and periods of 53 short-period eclipsing binaries with $P < 0.23$ d including 14 new eclipsing systems with periods $P < 0.22$ d by using SuperWASP da-

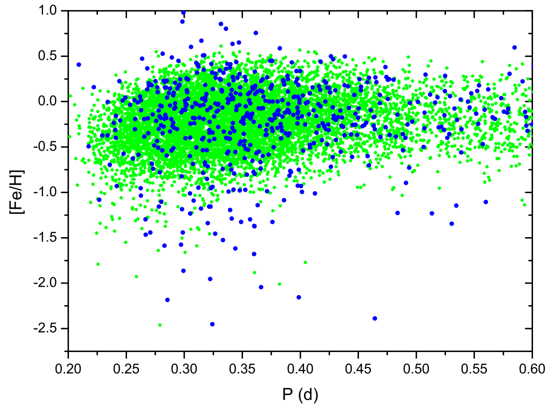

Fig. 14 The relation between orbital period (P) and metallicity [Fe/H] for EWs with $P < 0.6$ d. Symbols are the same as those in Figs. 3 and 7.

ta. They pointed out that the period distribution of contact binaries shows a sharp cut-off at a lower limit of around 0.22 d. Based on photometric data from the SDSS survey (York et al. 2000), Becker et al. (2011) found many M-type main-sequence eclipsing binaries including 28 M-dwarf contact binaries. Nefs et al. (2012) later detected 14 eclipsing binary candidates with orbital periods less than 0.22 d in the Wide-Field Camera (WFCAM) Transit Survey. Drake et al. (2014) investigated 367 ultra-short period binary candidates selected from 31 000 objects identified from Catalina Surveys. Thanks to these photometric surveys (e.g., SDSS, WFCAM Transit Survey, SuperWASP and Catalina Surveys), more and more close binaries with periods below the limit ($P < 0.22$ d) have been discovered that provide a good chance to investigate the short-period limit.

Contact binaries below the period limit have been found by several authors (e.g., Drake et al. 2014; Qian et al. 2015). Based on the spectroscopic and photometric analyses, Davenport et al. (2013) discovered SDSS J001641-000925 is an M-type contact binary system with a period of 0.19856 d. However, they pointed out that the period of the binary is decreasing rapidly and will be destroyed because of dynamical instability as predicted by Jiang et al. (2012). Qian et al. (2015) investigated the period variations of SDSS J001641–000925 and discovered that it is stable, indicating that it is the first M-type binary to be identified below the short-period limit. Qian et al. also found that there is a close-in stellar companion in the binary system. Later, Drake et al. (2014) spectroscopically confirmed the existence of M-dwarf+M-dwarf contact binary stars. Recently, many contact binaries near or below the period limit were detected based on follow-up observations and analyzing their light curves (see table 1 in Zhang & Qian 2020).

A large number of M-type main-sequence eclipsing binaries were detected by Becker et al. (2011) who determined $g-r$, $r-i$ and $i-z$ color indexes for those binary stars. The relations between the orbital period and these colors are displayed in Figure 12. As featured in the panels of the figure, there are period-color relations for short-period M-type binaries with periods shorter than 0.22 d, but no such relations for longer-period binary systems. By employing the least-squares method, the following equations

$$\begin{aligned} g-r &= 1.65(\pm0.16) - 2.5(\pm0.9)\times P \\ r-i &= 1.80(\pm0.30) - 5.6(\pm1.5)\times P \\ i-z &= 1.04(\pm0.16) - 3.3(\pm0.9)\times P, \end{aligned} \tag{4}$$

are determined. These period-color relations reveal that those short-period systems may be true M-dwarf contact binaries.

Early period distributions manifest a very sharp cut-off at around 0.22 d (e.g., Rucinski 1992, 2007). As the number of short-period EWs increases, the short-period cut-off in the period distribution given by Drake et al. (2014) is then less sharp. Based on 40 464 EWs collected in VSX by 2017 March 13, the period distribution constructed by Qian et al. (2017) reveals a lower limit for period at about 0.2 d. A new period distribution for short-period contact binaries with orbital periods shorter than 0.26 d is plotted in Figure 13. To construct the distribution, the data on 7118 objects with $P < 0.26$ in VSX are used. As displayed in the figure, the short-period cut-off is less sharp than that reported by Drake et al. (2014) and a short-period limit is lower than 0.2 d. Zhang & Qian (2020) analyzed the reason why contact binaries exhibit period-color and period-separation relations. They obtained a period cut-off at about 0.15 d theoretically by studying the correlation among physical parameters of contact binaries. This value is lower than all previously discovered and more and more contact binaries will be detected in the period range between 0.15 d and 0.2 d (Wang & Ip 2020).

Even though the short-period cut-off is now less sharp and contact binaries below 0.22 d have been found, the number of short-period contacts is also small. Low-mass dwarf stars are very common, but how they evolve into close binaries is poorly understood. The reason for the rarity of short-period contact binaries may be related to magnetic wind-driven AML mechanisms that become less efficient at short periods (Stepien 2006). As displayed in Figure 14, the gravitational accelerations of contact binaries near 0.2 d are very high, indicating that they are cool main-sequence stars with little evolution. However, their metallicity is lower than that of other contact systems, re-

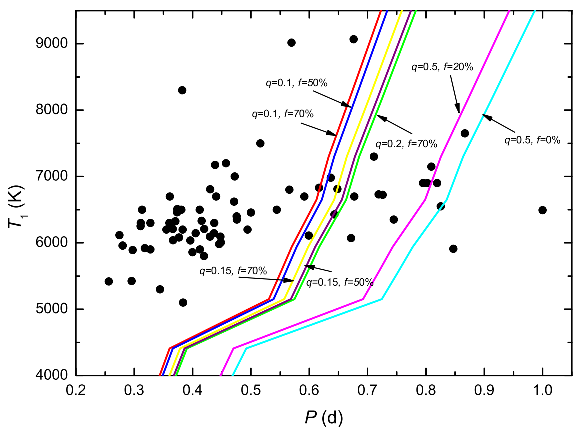

Fig. 15 The relation of the orbital period with the temperature for the primary component. Data come from Table 6. The colored solid lines mark the boundaries between the MSCBs and PMSCBs with different groups of key parameters. More details can be found in Sect. 6.

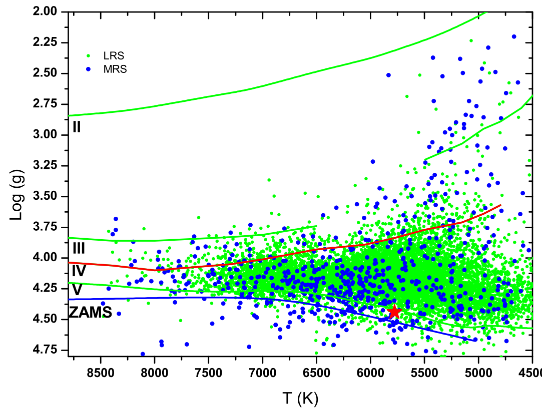

Fig. 16 The $\log g - T$ diagram for contact binary stars observed by LAMOST. Symbols are the same as those in Fig. 3. The position of the Sun is plotted as the red star. The green and red lines stand for the luminosity class range between II and V that are from Straizys & Kuriliene (1981). The blue line refers to the zero-age main sequence that is from Cox (2000).

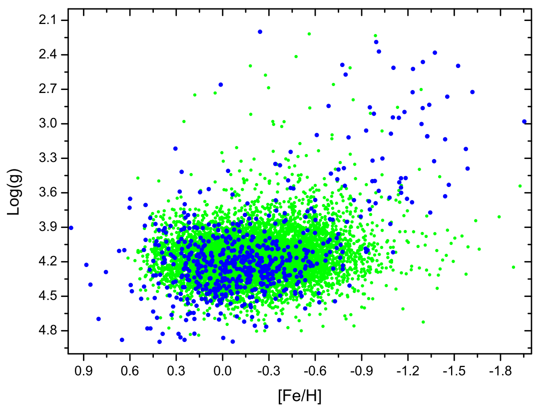

Fig. 17 Relation between the metallicity [Fe/H] and the gravitational acceleration $\log(g)$ for EWs with $P < 0.6$ d. Symbols are the same as those in Figs. 3, 7 and 14.

vealing that they are an old population (see Fig. 14). The accumulation of these binaries at the short orbital period around 0.2 d suggests that the wind-driven AML, leading to orbital period evolution, becomes less efficient at short periods. However, details of the process are still unclear. The increased number of short-period cool binaries provide us a chance to study the rarity of extremely short period contact binaries, and can reveal valuable information on the origin and evolution of contact binaries as well as on the formation and migration history of low-mass binary stars (Qian et al. 2014).

6 ADVANCED EVOLVED CONTACT BINARY SYSTEMS

Most contact binaries are thought to have main-sequence components. Typically, a contact binary with a temperature of 6000 K usually has $\log g = 4.30$. If the common logarithm of the gravitational acceleration for a similar primary component is less than 4.0, it should evolve off the main-sequence to the red giant branch (RGB). Such contact binaries could be called advanced evolved contact binaries (AECBs) or post-main-sequence contact binaries (PMSCBs). Figure 15 is the relation of period with temperature for some well-studied contact binaries. The solid lines are the boundaries between the main-sequence contact binaries (MSCBs) and AECBs. AECBs are to the right of the boundaries, indicating that their components have lower temperatures and larger radii. The mass ratio and fill-out factor both affect the boundaries. These boundaries were calculated as follows.

(1) For a given temperature of a main-sequence star, its mass (M_1) could be predicted (Allen 1977).

(2) For a given $\log g$, the radius could be calculated if the mass is known ($\log g = \log M/R^2 + 4.50$. For the Sun, $\log g = 4.50$).

(3) For a given mass ratio q, the mass of the secondary component (M_2) is determined if the mass of the primary one is known.

(4) For a given contact degree f, with given q in (3), the radius ratio r_1/r_2 is also determined by the Roche model. By utilizing the radius obtained in step (2), the separation A is determined. More details can be found in the

Table 7 Parameters of Some PMSCBs Observed by LAMOST DR7 in LSR

Name (1)	R.A. (2)	Dec. (3)	P (d) (4)	Times (5)	$\overline{T_{\rm eff}(K)}$ (6)	E_1 (7)	$\overline{\log(g)}$ (8)	E_2 (9)	$\overline{[\rm Fe/H]}$ (10)	E_3 (11)
ZALD 15	000111.24	+564340.7	0.282618	1	6950.06	42.69	3.741	0.070	0.175	0.040
ROTSE1 J000349.50+315316.0	000349.50	+315316.0	0.438080	1	6080.90	64.18	3.849	0.106	0.075	0.062
ASASSN-V J000438.42+333406.0	000438.42	+333406.0	0.677636	1	6862.53	191.81	3.797	0.303	0.034	0.179
CSS J000455.3+395050	000455.39	+395049.9	0.301548	1	5333.58	852.34	3.615	—	–0.767	0.790
WISE J000604.7+474228	000604.78	+474228.0	0.3196552	2	5467.89	123.57	3.593	0.146	–0.524	0.195
CSS J000715.7+253905	000715.77	+253905.8	0.276047	1	5544.52	321.67	3.756	0.508	–1.196	0.304
ASASSN-V J000736.91+364106.0	000736.91	+364106.0	0.322655	1	4995.81	44.16	3.497	0.073	–0.305	0.042
CSS J001820.9+393138	001820.97	+393138.8	0.3482964	3	5214.07	467.46	2.909	0.945	–0.957	0.432
CSS J001830.2+374744	001830.24	+374744.2	7.1878324	3	4799.41	93.25	2.981	0.154	–0.398	0.068
CSS J002250.5+370708	002250.54	+370708.0	0.30925	2	5256.31	203.92	3.690	0.776	–0.516	0.045
CSS J002352.4+410834	002352.43	+410834.1	0.309174	2	5610.84	22.27	3.443	0.144	–1.032	0.120
ASASSN-V J002516.91+434831.5	002516.91	+434831.5	0.720187	1	7496.95	243.66	3.819	0.402	0.250	0.233
WISE J003710.9+460020	003710.95	+460020.8	0.3619223	1	5670.29	225.91	3.666	0.356	–0.497	0.211
CSS J004219.7+400838	004219.78	+400838.8	0.329274	1	5644.14	376.94	3.724	0.612	–0.589	0.359
V0504 And	004500.35	+384356.1	0.6480	2	6793.24	23.02	3.881	0.013	0.303	0.054
V0508 And	004744.15	+360223.1	0.7752	1	6576.93	11.97	3.907	0.018	0.115	0.010
TYC 3659–550–1	005307.27	+545908.3	0.275862	1	6606.69	40.74	3.472	0.063	0.549	0.034
CSS J005333.3+145615	005333.37	+145615.3	0.305792	1	5209.74	576.26	3.459	0.925	–1.406	0.549
V0514 And	005453.20	+352803.0	0.36693	1	5743.70	179.03	3.753	0.281	–0.337	0.167
WISE J010202.9+521255	010202.95	+521255.2	0.6918993	1	7060.97	29.65	4.018	0.049	–0.043	0.028
CSS J010225.8+372027	010225.80	+372027.6	0.626532	3	7295.83	56.50	4.007	0.042	–0.018	0.030
CSS J010848.4+385911	010848.43	+385911.4	0.271512	2	5327.41	155.49	3.728	0.169	–0.804	0.158
CSS J010906.0+055229	010906.04	+055229.5	0.290955	1	5375.53	186.50	3.464	0.305	–0.548	0.178
CSS J011435.1+395617	011435.16	+395617.2	0.319182	1	5652.16	185.00	3.788	0.287	–0.077	0.171
CSS J011830.6+055957	011830.62	+055957.9	0.266248	1	4977.74	322.02	3.536	0.524	–1.158	0.307
NSVS 9167911	012140.45	+075011.0	1.1522	2	5506.39	100.26	3.743	0.167	–0.180	0.161
NSVS 3867879	012531.43	+480747.9	0.61084834	1	6883.36	24.85	3.952	0.041	0.256	0.023
VSX J012559.7+203404	012559.72	+203404.4	0.390176	2	5549.09	177.61	3.728	0.281	0.037	0.222
CSS J012944.3+441143	012944.32	+441143.3	0.7202021	1	7432.66	95.02	3.916	0.157	–0.226	0.091
CSS J013541.6+441517	013541.67	+441517.3	0.288172	1	5117.58	328.29	3.393	0.526	–0.730	0.312
CSS J013917.6+381416	013917.67	+381416.6	0.305082	1	5130.56	315.39	3.633	0.493	–0.576	0.293
WISE J013930.1+511022	013930.19	+511022.2	0.30502	1	5550.07	221.47	3.699	0.345	–0.554	0.205
CSS J014625.8+353911	014625.83	+353911.3	0.306908	1	5895.66	321.59	3.812	0.519	–0.598	0.306
WISE J014635.1+492329	014635.12	+492329.1	0.9934574	1	7093.14	81.81	3.928	0.135	–0.085	0.079
CSS J014730.9+374614	014730.97	+374614.2	0.344986	3	5988.97	125.90	3.854	0.441	–0.583	0.114
WISE J014937.2+471155	014937.20	+471156.0	0.6613124	1	7080.26	302.97	3.954	0.487	–0.195	0.288
WISE J015230.9+551621	015230.91	+551621.0	0.9102898	1	7201.48	31.14	3.910	0.051	0.002	0.030
WISE J015249.1+530023	015249.11	+530023.2	0.9828799	1	6885.57	28.10	3.901	0.046	0.099	0.027
WISE J015420.8+493511	015420.88	+493511.1	0.6821516	1	7181.06	156.61	3.990	0.249	0.072	0.147
WISE J015702.7+425528	015702.72	+425528.7	0.6122643	2	7455.79	79.71	4.006	0.062	–0.021	0.021
CSS J015841.2+392517	015841.22	+392517.1	0.264126	1	5269.99	298.30	3.447	0.463	–0.490	0.277
WISE J020146.4+551128	020146.46	+551128.9	0.8629935	1	6988.35	25.78	3.986	0.043	–0.181	0.024
V0802 And	020515.87	+412813.3	0.65552	1	7150.78	16.24	4.006	0.024	–0.018	0.013
CSS J020534.3+363228	020534.32	+363228.6	0.295862	2	5393.14	541.57	2.790	1.167	–0.845	0.218
V0575 And	022844.32	+372859.3	0.6780	1	7089.13	13.07	4.008	0.021	0.075	0.011
CSS J023122.2+133138	023122.25	+133138.2	0.285252	1	5003.60	190.70	3.565	0.299	–0.418	0.179
WISE J023347.4+482911	023347.40	+482911.9	0.9379914	1	6608.48	50.35	3.850	0.083	0.157	0.048
CSS J023611.9+260504	023611.94	+260504.4	0.320528	1	5706.18	318.69	3.771	0.515	–0.084	0.304
CSS J023806.7+150043	023806.78	+150043.0	0.29078	1	5412.57	226.82	3.676	0.358	–0.573	0.212
BEST F2_11600	024006.00	+521120.2	0.33177	1	4899.21	34.00	2.495	0.056	–0.180	0.032

paper of Liu et al. (2018), where they have introduced how to calculate the effective radius for each component with the Roche geometric model under the mass point condition.

(5) From steps (1) to (4), the critical T, M_1, M_2 and A were known. By applying Kepler's third law, the critical period can be calculated. Finally, the boundaries are obtained for a given $\log g$, q and f, just as Figure 15 shows.

The critical $\log g = 4.2$ was adopted when the temperature was lower than 5000 K, for which the value corresponds to a spectral type being later than K0V. This makes a jump in the theoretical boundary. The same situation could happen at a high temperature.

According to Figure 15, some contact binaries such as KIC 11097678, KIC 3104113, KIC 8539720 (Zola et al. 2017), KN Per (Goderya et al. 1997), II UMa (Zhou et al. 2016), TY Pup (Sarotsakulchai et al. 2018), V2388 Oph (Yakut et al. 2004), MW Pav (Alvarez et al. 2015) and V343 Ori (Yang 2009) should be PMSCBs. As we can see in Figures 4 and 8, LAMOST has found many EWs that are located below the right boundary of normal EWs. The contact binaries have lower temperature and longer orbital period and thus they are AECBs. The $\log g - T$ diagram for contact binary stars observed by LAMOST is shown in Figure 16. As displayed in the figure, some EWs are located above the IV line, indicating that they are subgiants or giants and thus are PMSCBs. Some of them are listed in Table 7.

The relation between the metallicity [Fe/H] and the the gravitational acceleration $\log(g)$ for EWs is plotted in Figure 17. As we can seen in the figure, evolved contact binaries (higher $\log(g)$) usually have lower metallicity, indicating that they are really old systems and have enough time to evolve into PMSCBs. In the post-main-sequence evolutionary stage, the radius of the primary component should expand. Eventually, the secondary component will be swallowed by the expanded shell of the primary component, causing a merger and producing a luminous red nova like V1309 Sco, the progenitor of which is composed of a giant with a mass of $1.52\,\mathrm{M}_{\odot}$ and a main-sequence companion with a mass of $0.16\,\mathrm{M}_{\odot}$ (e.g., Stępień 2011; Nandez et al. 2014). Hence, more attention should be paid to AECBs in the future.

7 CONCLUSIONS AND FUTURE WORKS

We review the progresses of the LAMOST spectroscopic survey on EWs since the investigation by Qian et al. (2017) and catalog stellar atmospheric parameters of 9149 EW-type contact binaries determined by low- and medium-resolution spectra from LAMOST. Those spectroscopic data can be applied during photometric solutions and big data of stellar parameters from the LAMOST survey provide important information for studying EWs. Then based on LAMOST data together with those acquired with many telescopes around the world, we focus on several groups of contact binaries, i.e., marginal contact binary systems, DLMCBs, systems near and below the short-period limit of contact binaries and AECB systems (Wang & Ip 2020).

We review the formation and classification of EW-type contact binary systems and a give new period distribution of EWs. The period-temperature relation is determined well by using the LAMOST data on normal EWs. EWs near the right border are marginal contact binaries, while those close to the left border are deep contact systems. They are at the beginning and at the final evolutionary stage of contact binary evolution. Contact binaries may be formed from mass-transferring semi-detached binaries or directly formed from short-period cool EAs through AML via magnetic braking. Objects beyond the borders of normal EWs on the period-temperature diagram are special targets or evolved contact binaries that need further investigation. The V361 Lyr-like semi-detached binaries are a group of mass-transferring systems that are very important for investigating the mass transfer and formation of EWs. However, only a few were detected to date.

DLMCBs were defined 15 years ago by Qian et al. (2005a) and they are at the end evolutionary stage of tidally-locked magnetic binaries. We collected the parameters of 76 DLMCBs and they show no obvious tendentious distribution for the $q - f$ relationship. It is found that the temperature difference is weakly correlated with the mass ratio and some DLMCBs are ascertained to have a large temperature difference, indicating that the energy transfer in the CCE does not only depend on the depth of CCE. The secondary components of these systems may be evolved and have higher intrinsic temperature. Some extremely low-mass ratio contact binaries have been detected which cannot be explained by the theory indicating that the physical properties and interior structure of contact binaries are unclear. Since there are still a lot of problems in contact binaries to solve, theoretical models cannot explain all the features well. It is necessary to utilize large sky surveys to search for more and more contact binaries that stay on key evolutionary phases. Based on the LAMOST data and follow-up observations, a lot of DLMCBs will be identified in the future.

Several photometric surveys and many detailed investigations have contributed to the detection of short-period EWs. The suspected short-period limit for contact binaries at about 0.22 d is not real at present. The period-color relation of M-type binaries reveals that there are contact binaries below the short-period limit. Several contact binaries with periods lower than 0.2 d have been discovered in recent years. A new period cut-off at around 0.15 d was determined indicating that more and more contact binaries with periods between 0.15 d and 0.2 d will be detected in the future. However, low-mass dwarf stars are very common, and the number of short-period contact binaries is still very small. How they form is an unsolved question in stellar astrophysics.

The theoretical boundaries of AECBs are given that depend on q and f. Moreover, some evolved contact binaries containing sub-giants or giants have been detected by the LAMOST survey. In these AECBs, the secondary components will be swallowed by the expanded shell of the primary ones. The CE will be ejected and the two components will be merging and producing a luminous red nova like V1309 Sco. Therefore, they provide a good opportunity to investigate the evolution of a CE and will evolve into some special targets. These post-contact systems need follow-up photometric and spectroscopic observations and detailed investigations in the future.

Contact binaries have the shortest orbital period and lowest angular momentum among main-sequence close binaries. More and more third components were detected in contact binary systems (e.g. Pribulla & Rucinski 2006; D'Angelo et al. 2006; Tokovinin et al. 2006; Rucinski et al. 2007). The third bodies of EWs are not considered in this paper. However, it was proposed that angular momentum can transfer from the central pair to the third body via the Kozai effect (Kozai 1962), which could cause the orbit of a detached binary to shrink in a short time scale, producing abundant contact binaries (e.g. Qian et al. 2007b, 2008a,b,c, 2009). More introductions and calculations of the formation and evolution of contact binaries stars can be found in some references such as Webbink (1976), Stepien (2006), Stępień (2011) and Eggleton (2012). New observations and investigations on the third bodies in EWs will help us to understand the formation and evolution of contact systems.

Acknowledgements This work is partly supported by the National Natural Science Foundation of China (Nos. 11933008, 11922306, 11773066 and 11903076) and the Open Project Program of the Key Laboratory of Optical Astronomy, National Astronomical Observatories, Chinese Academy of Sciences. New multi-color light curves of UV Mon were observed by the 1.0-m telescope administered by Yunnan Observatories. The Guo Shoujing Telescope (the Large Sky Area Multi-Object Fiber Spectroscopic Telescope, LAMOST) is a National Major Scientific Project built by the Chinese Academy of Sciences. Funding for the project has been provided by the National Development and Reform Commission. LAMOST is operated and managed by National Astronomical Observatories, Chinese Academy of Sciences. Spectroscopic observations used in the paper were obtained with LAMOST from 2011 October 24 to 2019 June 8.

References

Acerbi, F., Barani, C., & Martignoni, M. 2014, New Astron., 31, 1
Allen, K. W. 1977, Astrophysical quantities. (Translated from the 3. revised and suppl. English edition. Moskva: Mir)
Alvarez, G. E., Sowell, J. R., Williamon, R. M., & Lapasset, E. 2015, PASP, 127, 742
Arbutina, B. 2007, MNRAS, 377, 1635
Arbutina, B. 2009, MNRAS, 394, 501
Bakos, G., Noyes, R. W., Kovács, G., et al. 2004, PASP, 116, 266
Becker, A. C., Bochanski, J. J., Hawley, S. L., et al. 2011, ApJ, 731, 17
Binnendijk, L. 1970, Vistas in Astronomy, 12, 217
Borucki, W. J., Koch, D., Basri, G., et al. 2010, Science, 327, 977
Broens, E. 2013, MNRAS, 430, 3070
Cai, J.-T., Yu, Y.-X., Hu, K., & Xiang, F.-Y. 2019, RAA (Research in Astronomy and Astrophysics), 19, 106
Caton, D., Gentry, D. R., Samec, R. G., et al. 2019, PASP, 131, 054203
Cheng, Y., Zhang, L.-y., Han, X. L., et al. 2019, AJ, 158, 193
Christopoulou, P. E., Parageorgiou, A., & Chrysopoulos, I. 2011, AJ, 142, 99
Csák, B., Kiss, L. L., Vinkó, J., & Alfaro, E. J. 2000, A&A, 356, 603
Şenavcı, H. V., Nelson, R. H., Özavcı, İ., Selam, S. O., & Albayrak, B. 2008, New Astron., 13, 468
D'Angelo, C., van Kerkwijk, M. H., & Rucinski, S. M. 2006, AJ, 132, 650
Davenport, J. R. A., Becker, A. C., West, A. A., et al. 2013, ApJ, 764, 62
Drake, A. J., Djorgovski, S. G., Mahabal, A., et al. 2009, ApJ, 696, 870
Drake, A. J., Graham, M. J., Djorgovski, S. G., et al. 2014, ApJS, 213, 9
Duerbeck, H. W., & Karimie, M. T. 1979, Information Bulletin on Variable Stars, 1617, 1
Eggen, O. J. 1967, MmRAS, 70, 111
Eggleton, P. 2006, Evolutionary Processes in Binary and Multiple Stars (Cambridge, UK: Cambridge Univ. Press)
Eggleton, P. P. 2012, Journal of Astronomy and Space Sciences, 29, 145
Essam, A., Saad, S. M., Nouh, M. I., et al. 2010, New Astron., 15, 227
Ferreira, T., Saito, R. K., Minniti, D., et al. 2019, MNRAS, 486, 1220
Flannery, B. P. 1976, ApJ, 205, 217
Gazeas, K. D., & Niarchos, P. G. 2006, MNRAS, 370, L29
Gazeas, K. D., Baran, A., Niarchos, P., et al. 2005, Acta Astronomica, 55, 123
Gazeas, K., & Stępień, K. 2008, MNRAS, 390, 1577
Goderya, S. N., Leung, K. C., & Schmidt, E. G. 1996, Ap&SS, 246, 291
Goderya, S. N., Leung, K. C., & Schmidt, E. G. 1997, Ap&SS, 254, 295
Gu, S.-h., Chen, P.-s., Choy, Y.-k., et al. 2004, A&A, 423, 607
Guinan, E. F., & Bradstreet, D. H. 1988, in NATO Advanced Science Institutes (ASI) Series C, 241, eds. A. K. Dupree, & M. T. V. T. Lago, 345
Gürol, B., Gürsoytrak, S. H., & Bradstreet, D. H. 2015, NewA, 39, 9
Hilditch, R. W., & King, D. J. 1986, MNRAS, 223, 581
Hilditch, R. W., King, D. J., & McFarlane, T. M. 1988, MNRAS, 231, 341
Hilditch, R. W., Collier Cameron, A., Hill, G., Bell, S. A., & Harries, T. J. 1997, MNRAS, 291, 749
Howell, S. B., Sobeck, C., Haas, M., et al. 2014, PASP, 126, 398
Hu, K., Jiang, Z.-H., Yu, Y.-X., & Xiang, F.-Y. 2018, New Astron., 62, 20

Hu, K., Chen, K., Xiang, F.-Y., Yu, Y.-X., & Zhao, E.-G. 2019, AJ, 158, 104
Hut, P. 1980, A&A, 92, 167
Jiang, D., Han, Z., Wang, J., Jiang, T., & Li, L. 2010, MNRAS, 405, 2485
Jiang, D., Han, Z., Ge, H., Yang, L., & Li, L. 2012, MNRAS, 421, 2769
Kaluzny, J. 1990, AJ, 99, 1207
Kandulapati, S., Devarapalli, S. P., & Pasagada, V. R. 2015, MNRAS, 446, 510
Kang, Y. W., Kim, H.-i., Lee, W.-B., & Oh, K.-D. 2001, MNRAS, 325, 707
Kjurkchieva, D. P., Popov, V. A., Vasileva, D. L., & Petrov, N. I. 2017, RMxAA, 53, 235
Kjurkchieva, D. P., Popov, V. A., & Petrov, N. I. 2019, AJ, 158, 186
Kopal, Z. 1959, Close Binary Systems (The International Astrophysics Series, London: Chapman & Hall)
Kozai, Y. 1962, AJ, 67, 591
Lee, J. W., Park, J.-H., Hong, K., Kim, S.-L., & Lee, C.-U. 2014, AJ, 147, 91
Li, K., & Qian, S. B. 2013, New Astron., 21, 46
Li, L., Liu, Q., Zhang, F., & Han, Z. 2001, AJ, 121, 1091
Li, L., & Zhang, F. 2006, MNRAS, 369, 2001
Li, L., Zhang, F., Han, Z., Jiang, D., & Jiang, T. 2008, MNRAS, 387, 97
Li, X.-Z., & Liu, L. 2020a, New Astron., 81, 101445
Li, X. Z., Liu, L., 2020b, in prepared
Li, X.-Z., Liu, L., & Zhang, X.-D. 2020, PASJ, 72, 66
Liao, W. P., Qian, S. B., Soonthornthum, B., et al. 2017, PASP, 129, 124204
Liao, W. P., & Sarotsakulchai, T. 2019, PASP, 131, 014202
Lipari, S. L., & Sistero, R. F. 1986, MNRAS, 220, 883
Lipari, S. L., & Sistero, R. F. 1987, AJ, 94, 792
Lister, T. A. 2009, in American Institute of Physics Conference Series, 1094, 15th Cambridge Workshop on Cool Stars, Stellar Systems, and the Sun, ed. E. Stempels, 688
Liu, L., Chen, W. P., Na, W. W., et al. 2014, New Astron., 31, 60
Liu, L., Qian, S.-B., Soonthornthum, B., et al. 2015, PASJ, 67, 74
Liu, L., Qian, S., Zhu, L., et al. 2017, New Astron., 51, 1
Liu, L., Qian, S. B., & Xiong, X. 2018, MNRAS, 474, 5199
Liu, C., Fu, J., Shi, J., et al. 2020a, arXiv e-prints, arXiv:2005.07210
Liu, N.-P., Sarotsakulchai, T., Rattanasoon, S., & Zhang, B. 2020b, arXiv:2006.12711
Long, L., Zhang, L.-Y., Han, X. L., et al. 2019, MNRAS, 487, 5520
Lu, H.-p., Zhang, L.-y., Han, X. L., Pi, Q.-f., & Wang, D.-m. 2017, New Astron., 51, 59
Lu, W., & Rucinski, S. M. 1999, AJ, 118, 515
Lu, W., Rucinski, S. M., & Ogłoza, W. 2001, AJ, 122, 402
Lucy, L. B. 1968a, ApJ, 153, 877
Lucy, L. B. 1968b, ApJ, 151, 1123
Lucy, L. B. 1973, Ap&SS, 22, 381
Lucy, L. B. 1976, ApJ, 205, 208
Luo, A. L., Zhang, H.-T., Zhao, Y.-H., et al. 2012, RAA (Research in Astronomy and Astrophysics), 12, 1243
Luo, A. L., Zhao, Y.-H., Zhao, G., et al. 2015, RAA (Research in Astronomy and Astrophysics), 15, 1095
McLean, B. J., & Hilditch, R. W. 1983, MNRAS, 203, 1
Milano, L., Barone, F., Mancuso, S., Russo, G., & Vittone, A. A. 1989, A&A, 210, 181
Milone, E. F., Stagg, C. R., Sugars, B. A., et al. 1995, AJ, 109, 359
Mochnacki, S. W. 1981, ApJ, 245, 650
Mochnacki, S. W., & Whelan, J. A. J. 1973, A&A, 25, 249
Na, W. W., Qian, S. B., Zhang, L., et al. 2014, New Astron., 30, 105
Nandez, J. L. A., Ivanova, N., & Lombardi, J. C., J. 2014, ApJ, 786, 39
Nefs, S. V., Birkby, J. L., Snellen, I. A. G., et al. 2012, MNRAS, 425, 950
Nelson, R. H., Milone, E. F., van Leeuwen, J., et al. 1995, AJ, 110, 2400
Norton, A. J., Payne, S. G., Evans, T., et al. 2011, A&A, 528, A90
Oh, K.-D., Kim, H.-I., & Lee, W.-B. 1997, Journal of Astronomy and Space Sciences, 14, 33
Paczyński, B., Szczygieł, D. M., Pilecki, B., & Pojmański, G. 2006, MNRAS, 368, 1311
Palaversa, L., Ivezić, Ž., Eyer, L., et al. 2013, AJ, 146, 101
Pepper, J., Kuhn, R. B., Siverd, R., James, D., & Stassun, K. 2012, PASP, 124, 230
Pi, Q.-f., Zhang, L.-y., Bi, S.-l., et al. 2017, AJ, 154, 260
Pojmanski, G. 1997, Acta Astronomica, 47, 467
Pojmanski, G., Pilecki, B., & Szczygiel, D. 2005, Acta Astronomica, 55, 275
Pollacco, D. L., Skillen, I., Collier Cameron, A., et al. 2006, PASP, 118, 1407
Pribulla, T., Chochol, D., Vanko, M., & Parimucha, S. 2002, Information Bulletin on Variable Stars, 5258, 1
Pribulla, T., & Rucinski, S. M. 2006, AJ, 131, 2986
Pribulla, T., Rucinski, S. M., Lu, W., et al. 2006, AJ, 132, 769
Pribulla, T., Rucinski, S. M., Conidis, G., et al. 2007, AJ, 133, 1977
Pribulla, T., & Rucinski, S. M. 2008, MNRAS, 386, 377
Pribulla, T., Vanko, M., & Hambalek, L. 2009a, Information Bulletin on Variable Stars, 5886, 1
Pribulla, T., Rucinski, S. M., DeBond, H., et al. 2009b, AJ, 137, 3646
Pribulla, T., Rucinski, S. M., Blake, R. M., et al. 2009c, AJ, 137, 3655
Pych, W., Rucinski, S. M., DeBond, H., et al. 2004, AJ, 127, 1712
Qian, S. 2001a, MNRAS, 328, 635

Qian, S. 2001b, MNRAS, 328, 914
Qian, S. 2002, MNRAS, 336, 1247
Qian, S. 2003, MNRAS, 342, 1260
Qian, S. B., & Yang, Y. G. 2004, AJ, 128, 2430
Qian, S. B., Yang, Y. G., Soonthornthum, B., et al. 2005a, AJ, 130, 224
Qian, S. B., Zhu, L. Y., Soonthornthum, B., et al. 2005b, AJ, 130, 1206
Qian, S., & Yang, Y. 2005, MNRAS, 356, 765
Qian, S. B., Liu, L., Soonthornthum, B., Zhu, L. Y., & He, J. J. 2006a, AJ, 131, 3028
Qian, S. B., Liu, L., Soonthornthum, B., Zhu, L. Y., & He, J. J. 2007a, AJ, 134, 1475
Qian, S., Yang, Y., Zhu, L., He, J., & Yuan, J. 2006b, Ap&SS, 304, 25
Qian, S. B., Yuan, J. Z., Liu, L., et al. 2007b, MNRAS, 380, 1599
Qian, S. B., He, J. J., Liu, L., Zhu, L. Y., & Liao, W. P. 2008a, AJ, 136, 2493
Qian, S. B., He, J. J., Soonthornthum, B., et al. 2008b, AJ, 136, 1940
Qian, S.-B., He, J.-J., & Xiang, F.-Y. 2008c, PASJ, 60, 77
Qian, S. B., Liu, L., & Zhu, L. Y. 2009, PASA, 26, 7
Qian, S. B., Liu, L., Zhu, L. Y., et al. 2011, AJ, 141, 151
Qian, S. B., Liu, N. P., Li, K., et al. 2013, ApJS, 209, 13
Qian, S. B., Jiang, L. Q., Zhu, L. Y., et al. 2014, Contributions of the Astronomical Observatory Skalnate Pleso, 43, 290
Qian, S. B., Jiang, L. Q., Fernández Lajús, E., et al. 2015, ApJL, 798, L42
Qian, S.-B., He, J.-J., Zhang, J., et al. 2017, RAA (Research in Astronomy and Astrophysics), 17, 087
Qian, S. B., Zhang, J., He, J. J., et al. 2018, ApJS, 235, 5
Rasio, F. A. 1995, ApJL, 444, L41
Richter, G. A., & Andronov, I. L. 1986, Zentralinstitut fuer Astrophysik Sternwarte Sonneberg Mitteilungen ueber Veraenderliche Sterne, 11, 27
Robertson, J. A., & Eggleton, P. P. 1977, MNRAS, 179, 359
Rucinski, S. M. 1985, Contact Binaries: Observational Properties, eds. J. E. Pringle, & R. A. Wade, Interacting Binary Stars, eds. J. E. Pringle, & R. A. Wade, 85
Rucinski, S. M. 1986, in IAU Symposium, 118, Instrumentation and Research Programmes for Small Telescopes, eds. J. B. Hearnshaw, & P. L. Cottrell, 159
Rucinski, S. M. 1992, AJ, 103, 960
Rucinski, S. M. 1998, AJ, 116, 2998
Rucinski, S. M., & Lu, W. 1999, AJ, 118, 2451
Rucinski, S. M., Lu, W., & Mochnacki, S. W. 2000, AJ, 120, 1133
Rucinski, S. M., Lu, W., Mochnacki, S. W., Ogłoza, W., & Stachowski, G. 2001, AJ, 122, 1974
Rucinski, S. M., Lu, W., Capobianco, C. C., et al. 2002, AJ, 124, 1738
Rucinski, S. M., Capobianco, C. C., Lu, W., et al. 2003, AJ, 125, 3258
Rucinski, S. M., Pych, W., Ogłoza, W., et al. 2005, AJ, 130, 767
Rucinski, S. M. 2007, MNRAS, 382, 393
Rucinski, S. M., Pribulla, T., & van Kerkwijk, M. H. 2007, AJ, 134, 2353
Rucinski, S. M., Pribulla, T., Mochnacki, S. W., et al. 2008, AJ, 136, 586
Rucinski, S. M. 2015, AJ, 149, 49
Samec, R. G., Labadorf, C. M., Hawkins, N. C., Faulkner, D. R., & Van Hamme, W. 2011, AJ, 142, 117
Samus', N. N., Kazarovets, E. V., Durlevich, O. V., Kireeva, N. N., & Pastukhova, E. N. 2017, Astronomy Reports, 61, 80
Sarotsakulchai, T., Qian, S. B., Soonthornthum, B., et al. 2018, AJ, 156, 199
Shi, X.-D., Qian, S.-B., Li, L.-J., Na, W.-W., & Zhou, X. 2020, RAA (Research in Astronomy and Astrophysics), 20, 096
Shobbrook, R. R., & Zola, S. 2006, Ap&SS, 304, 43
Siwak, M., Zola, S., & Koziel-Wierzbowska, D. 2010, Acta Astronomica, 60, 305
Sriram, K., Malu, S., Choi, C. S., & Vivekananda Rao, P. 2016, AJ, 151, 69
Stępień, K. 2009, MNRAS, 397, 857
Stępień, K. 2011, A&A, 531, A18
Stepien, K. 2006, Acta Astronomica, 56, 199
Stępień, K. 2011, Acta Astronomica, 61, 139
Stępień, K., & Kiraga, M. 2013, Acta Astronomica, 63, 239
Szalai, T., Kiss, L. L., Mészáros, S., Vinkó, J., & Csizmadia, S. 2007, A&A, 465, 943
Terrell, D., & Nelson, R. H. 2014, ApJ, 783, 35
Tian, X.-M., & Chang, L.-F. 2020, PASA, 37, e031
Tokovinin, A., Thomas, S., Sterzik, M., & Udry, S. 2006, A&A, 450, 681
Twigg, L. W. 1979, MNRAS, 189, 907
Van Hamme, W., Samec, R. G., Gothard, N. W., et al. 2001, AJ, 122, 3436
Virnina, N. A. 2013, Astronomical and Astrophysical Transactions, 28, 57
Wadhwa, S. S. 2005, Ap&SS, 300, 329
Wadhwa, S. S. 2006, Ap&SS, 301, 195
Wang, J. J., Jiang, L. Q., Zhang, B., Zhao, S. Q., & Yu, J. 2017, PASP, 129, 124202
Wang, J. X., & Ip, W.-H. 2020, RAA (Research in Astronomy and Astrophysics), 20, 157
Wang, K. 2017, RAA (Research in Astronomy and Astrophysics), 17, 112
Watson, C. L., Henden, A. A., & Price, A. 2006, Society for Astronomical Sciences Annual Symposium, 25, 47
Webbink, R. F. 1976, ApJ, 209, 829
Webbink, R. F. 2003, in Astronomical Society of the Pacific Conference Series, 293, 3D Stellar Evolution, eds. S. Turcotte, S. C. Keller, & R. M. Cavallo, 76
Wolf, M., & Kučáková, H. 2020, New Astron., 80, 101415
Woźniak, P. R., Vestrand, W. T., Akerlof, C. W., et al. 2004, AJ, 127, 2436

Wu, Y., Du, B., Luo, A., Zhao, Y., & Yuan, H. 2014, in IAU Symposium, 306, Statistical Challenges in 21st Century Cosmology, eds. A. Heavens, J.-L. Starck, & A. Krone-Martins, 340
Wu, Y., Luo, A. L., Li, H.-N., et al. 2011, RAA (Research in Astronomy and Astrophysics), 11, 924
Yakut, K., Kalomeni, B., & İbanoğlu, C. 2004, A&A, 417, 725
Yakut, K., & Eggleton, P. P. 2005, ApJ, 629, 1055
Yang, Y., & Liu, Q. 2003, New Astron., 8, 465
Yang, Y. G., Qian, S. B., & Zhu, L. Y. 2005, AJ, 130, 2252
Yang, Y. 2008, Ap&SS, 314, 151
Yang, Y. G. 2009, PASP, 121, 699
Yang, Y. G., Qian, S. B., Zhu, L. Y., & He, J. J. 2009, AJ, 138, 540
Yang, Y. G., Qian, S. B., & Soonthornthum, B. 2012, AJ, 143, 122
Yang, Y. G., Qian, S. B., Zhang, L. Y., Dai, H. F., & Soonthornthum, B. 2013, AJ, 146, 35
Yang, Y.-G., & Qian, S.-B. 2015, AJ, 150, 69
Yıldız, M. 2014, MNRAS, 437, 185
Yildiz, M., & Doğan, T. 2013, MNRAS, 430, 2029
York, D. G., Adelman, J., Anderson, John E., J., et al. 2000, AJ, 120, 1579
Yu, Y.-X., Xiang, F.-Y., & Xiao, T.-Y. 2015, PASJ, 67, 42
Yue, Q., Zhang, L.-Y., Han, X.-M. L., et al. 2019, RAA (Research in Astronomy and Astrophysics), 19, 097
Zhang, J., Qian, S.-B., Wu, Y., & Zhou, X. 2019, ApJS, 244, 43
Zhang, L., Zhu, Z., Yue, Q., et al. 2020a, MNRAS, 491, 6065
Zhang, X.-D., Qian, S.-B., & Liao, W.-P. 2020b, MNRAS, 492, 4112
Zhang, X.-D., & Qian, S.-B. 2020, MNRAS, 497, 3493
Zhao, G., Zhao, Y.-H., Chu, Y.-Q., Jing, Y.-P., & Deng, L.-C. 2012, RAA (Research in Astronomy and Astrophysics), 12, 723
Zhou, X., Qian, S. B., Liao, W. P., et al. 2015, AJ, 150, 83
Zhou, X., Qian, S. B., Zhang, J., Zhang, B., & Kreiner, J. 2016, AJ, 151, 67
Zhu, L., & Qian, S. 2006, MNRAS, 367, 423
Zhu, L. Y., Qian, S. B., Soonthornthum, B., & Yang, Y. G. 2005, AJ, 129, 2806
Zhu, L. Y., Qian, S. B., Zola, S., & Kreiner, J. M. 2009, AJ, 137, 3574
Zhu, L. Y., Qian, S. B., Soonthornthum, B., He, J. J., & Liu, L. 2011, AJ, 142, 124
Zhu, L. Y., Zejda, M., Mikulášek, Z., et al. 2012, AJ, 144, 37
Zhu, L. Y., Qian, S. B., Soonthornthum, B., et al. 2014, AJ, 147, 42
Zhu, L.-Y., Zhao, E.-G., & Zhou, X. 2016, RAA (Research in Astronomy and Astrophysics), 16, 68
Zola, S., Rucinski, S. M., Baran, A., et al. 2004, Acta Astronomica, 54, 299
Zola, S., Baran, A., Debski, B., & Jableka, D. 2017, MNRAS, 466, 2488